1

FUNDAMENTALS OF PLANAR TRANSMISSION LINES

1.1 PLANAR TRANSMISSION LINES, DISTRIBUTED CIRCUITS, AND ARTIFICIAL TRANSMISSION LINES

In radiofrequency (RF) and microwave engineering, transmission lines are two-port networks used to transmit signals, or power, between two distant points (the source and the load) in a guided (in contrast to radiated) way. There are many types of transmission lines. Probably, the most well-known transmission line (at least for nonspecialists in RF and microwave engineering) is the coaxial line (Fig. 1.1), which consists of a pair of concentric conductors separated by a dielectric, and is typically used to feed RF/microwave components and to connect them to characterization and test equipment. Other planar transmission lines are depicted in Figure 1.2. There are many textbooks partially or entirely focused on transmission lines and their RF and microwave applications [1–8]. The author recommends these books to those readers interested in the topic of the present book (artificial transmission lines), which are not familiar with conventional (or ordinary) transmission lines. Nevertheless, the fundamentals of planar transmission lines are considered in this chapter for completeness and for better comprehension of the following chapters. As long as waveguides (and even optical fibers) do also carry electromagnetic (EM) waves and EM energy between two points, they can also be considered transmission lines. However, this book is entirely devoted to planar structures; and for this reason, waveguides are out of the scope of this chapter.

Artificial Transmission Lines for RF and Microwave Applications, First Edition. Ferran Martín.

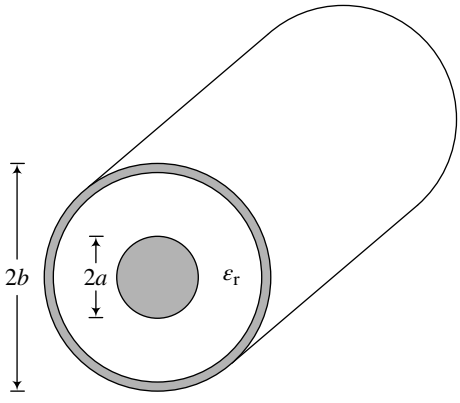

FIGURE 1.1 Perspective three-dimensional view of a coaxial transmission line. The relevant geometry parameters of the line are indicated, and ε_r is the relative permittivity (or dielectric constant) of the dielectric material.

Obviously, there are not transmission lines in natural form.[1] Transmission lines must be fabricated in order to satisfy certain requirements or specifications; in this sense, they are actually artificial (i.e., man-made) structures. However, the term *artificial transmission line* is restricted to a specific type of transmission lines, to distinguish them from the conventional ones.[2] Before discussing the definition and scope of the term *artificial transmission line*, let us now point out the different approaches for the study of planar (conventional) transmission lines. If the physical length of the transmission line is much smaller than the wavelength of the transmitted signals, the voltages and currents in the line are uniform, that is, they do not depend on the position in the line.[3] Under these conditions, the voltages and currents are dictated by the Kirchhoff's current and voltage laws and by the terminal equations of the lumped elements present at the input and output ports of the line, or at any position in the line. This is the so-called lumped element approach, which is generally valid up to about 100 MHz, or even further for planar structures (or circuits) including transmission lines not exceeding the typical sizes of printed circuit boards or PCBs (i.e., various centimeters). At higher frequencies, typically above 1 GHz, the finite propagation velocity of the transmitted signals (of the order of the speed of light) gives rise to variations of voltage and current along the lines, and the lumped circuit approach is no longer valid. At this regime, transmission lines can be analyzed by means of field theory, from Maxwell's equations. However, most planar transmission lines can alternatively be studied and described by means of an intermediate approach between lumped circuits and field equations: the distributed circuit approach. Indeed, for

[1] Exceptions to this are, for instance, the axons, which transmit nerve signals in brain neurons.
[2] Conventional (or ordinary) transmission lines are uniform along the propagation direction (see Fig. 1.2).
[3] Strictly speaking, this is true if losses are negligible. The effects of losses in transmission lines will be discussed later in detail.

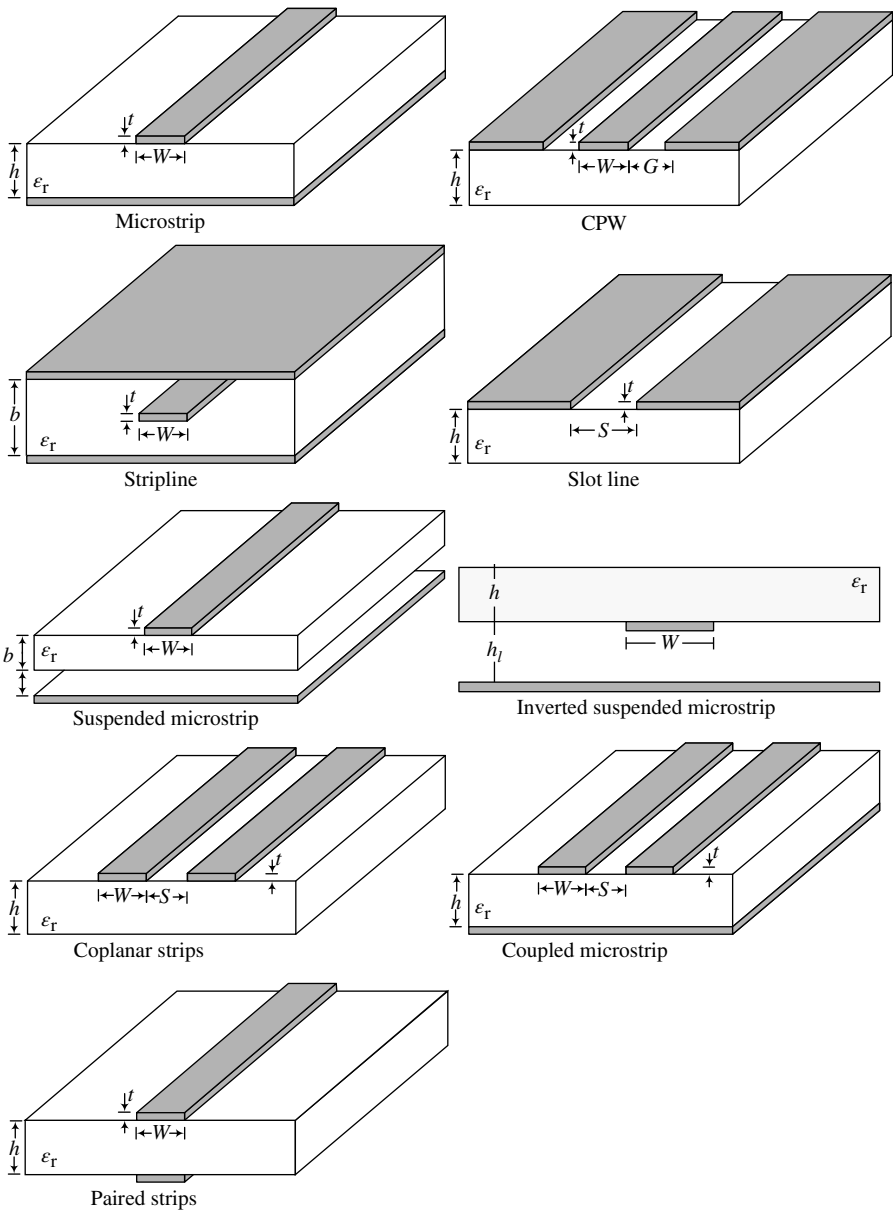

FIGURE 1.2 Perspective three-dimensional view of the indicated planar transmission lines, and relevant geometry parameters. These transmission lines are used for the implementation of distributed circuits, where the shape and transverse dimensions (W, S, G) of the line (or set of lines and stubs) are determined in order to obtain the required line functionality.

transverse electric and magnetic (TEM),[4] or quasi-TEM, wave propagation in planar transmission lines (i.e., the fundamental modes), there is a link between the results inferred from the distributed analysis and field theory. Nevertheless, this connection is discussed and treated in Appendix A, since it is not necessary to understand the contents of the present and the next chapters.

The most intriguing aspect of transmission lines operating at microwave frequencies and beyond is the fact that such lines can replace lumped elements, such as capacitances and inductances, in planar circuits, thus avoiding the use of lumped components which increase cost and circuit complexity. Hence, in RF and microwave engineering, transmission lines are not only of interest for signal or power transmission, but they are also key elements for microwave device and component design on the basis of the distributed approach. Thus, the constituent building blocks of distributed circuits are transmission lines and stubs,[5] which are implemented by simply etching metallic patterns on a microwave substrate (such patterns define a set of transmission lines and stubs providing certain functionality).

Distributed circuits are typically low cost since they are implemented in planar technology. However, the design flexibility, performance, or functionality of planar microwave circuits can be enhanced (and/or their dimensions can be reduced) by loading the lines with reactive elements (not necessarily planar),[6] or by breaking the uniformity of the lines in the direction of propagation, or by considering specific arrangements able to provide certain advantages as compared to ordinary lines. In the context of this book, the term *artificial transmission line* is used to designate these lines with superior characteristics, and to distinguish them from their conventional counterparts (ordinary lines). Hence, notice that the term *artificial transmission line* is not only restricted to designate artificial structures mimicking the behavior of ordinary lines (e.g., an LC ladder network or a capacitively loaded line acting as a slow wave transmission line).[7] In this book, the definition of *artificial transmission line* is

[4] Transmission lines supporting TEM modes require at least two conductors separated by a uniform (homogeneous) dielectric, and the electric and magnetic field lines must be entirely contained in such dielectric. In such modes, the electric and magnetic field components in the direction of propagation are null. A coaxial line is an example of transmission line that supports TEM modes. Microstrip and CPW transmission lines (see Fig. 1.2) are nonhomogeneous open lines, and hence do not support pure TEM modes, but quasi-TEM modes.

[5] Stubs are short- or open-circuit transmission line sections, shunt or series connected to another transmission line, intended to produce a pure reactance at the attachment point, for the frequency of interest.

[6] Notice that this loading refers to line loading along its length, not at the output port (as considered in Section 1.3 in reference to ordinary lines). A line with a load at its output port is usually referred to as terminated line.

[7] Artificial lines that mimic the behavior of ordinary lines are sometimes referred to as synthetic lines. Synthetic lines can be implemented by means of lumped, semilumped, and/or distributed components (combination of transmission lines and stubs). Synthetic lines purely based on the distributed approach (e.g., stub-loaded lines) are out of the scope of this book since they are indeed implemented by combining ordinary lines. Other artificial lines that can be considered to belong to the category of synthetic lines (e.g., capacitively loaded lines) are included in this book; but obviously, it is not possible to include all the realizations of synthetic lines reported in the literature. Artificial lines able to provide further functionalities than ordinary lines (e.g., metamaterial transmission lines with multiband functionality) are not considered to be synthetic transmission lines.

very broad and roughly covers all those lines that cannot be considered ordinary lines. Nevertheless, in many applications of artificial transmission lines, these lines simply replace ordinary lines, and the design approach of microwave circuits based on such artificial lines is similar to the one for ordinary lines, based on the control of the main line parameters. Therefore, in the next subsections, we will focus the attention on the study and analysis of ordinary lines, including the main transmission line parameters, reflections at the source and load (mismatching), losses in transmission lines, a comparative analysis of the most used planar transmission lines, and examples of applications. Most of these contents will be useful in the following chapters. Other useful contents for this chapter and chapters that follow (and in general for RF/microwave engineering), such as the Smith Chart and the scattering S-matrix, are included for completeness in Appendix B and C, respectively.

1.2 DISTRIBUTED CIRCUIT ANALYSIS AND MAIN TRANSMISSION LINE PARAMETERS

Planar transmission lines can be described by cascading the lumped element two-port network unit cell depicted in Figure 1.3, corresponding to an infinitesimal piece of the transmission line of length Δz, and C', L', R', and G' are the line capacitance, line inductance, line resistance, and line conductance per unit length, respectively. R' is related to conductor losses, whereas G' accounts for dielectric losses. From Kirchhoff's circuit laws applied to the network of Figure 1.3, the following equations are obtained:

$$v(z,t) - R'\Delta z \cdot i(z,t) - L'\Delta z \frac{\partial i(z,t)}{\partial t} - v(z+\Delta z,t) = 0 \tag{1.1a}$$

$$i(z,t) - G'\Delta z \cdot v(z+\Delta z,t) - C'\Delta z \frac{\partial v(z+\Delta z,t)}{\partial t} - i(z+\Delta z,t) = 0 \tag{1.1b}$$

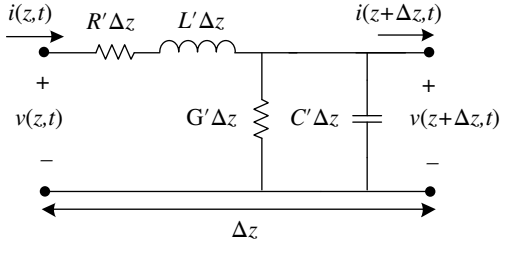

FIGURE 1.3 Lumped element equivalent circuit model (unit cell) of an ordinary transmission line.

By dividing these equations by Δz, and taking the limit as $\Delta z \to 0$, it follows:

$$\frac{\partial v(z,t)}{\partial z} = -R'i(z,t) - L'\frac{\partial i(z,t)}{\partial t} \tag{1.2a}$$

$$\frac{\partial i(z,t)}{\partial z} = -G'v(z,t) - C'\frac{\partial v(z,t)}{\partial t} \tag{1.2b}$$

Equations 1.2 are known as the telegrapher equations. If we now consider sinusoidal steady-state conditions (i.e., $v(z, t) = V(z)\cdot e^{j\omega t}$ and $i(z, t) = I(z)\cdot e^{j\omega t}$), the time variable in the previous equations can be ignored:

$$\frac{dV(z)}{dz} = -(R' + j\omega L')I(z) \tag{1.3a}$$

$$\frac{dI(z)}{dz} = -(G' + j\omega C')V(z) \tag{1.3b}$$

and the well-known wave equations result

$$\frac{d^2V(z)}{dz^2} - \gamma^2 V(z) = 0 \tag{1.4a}$$

$$\frac{d^2I(z)}{dz^2} - \gamma^2 I(z) = 0 \tag{1.4b}$$

where $\gamma = \alpha + j\beta$ is the complex propagation constant, given by

$$\gamma = \sqrt{(R' + j\omega L')(G' + j\omega C')} \tag{1.5}$$

and α and β are the attenuation constant and the phase constant, respectively. Notice that if conductor and dielectric losses can be neglected ($R' = G' = 0$), $\alpha = 0$, and the phase constant is proportional to the angular frequency and given by

$$\beta = \omega\sqrt{L'C'} \tag{1.6}$$

The general solutions of the wave equations are traveling waves of the form:

$$V(z) = V_o^+ e^{-\gamma z} + V_o^- e^{\gamma z} \tag{1.7a}$$

$$I(z) = I_o^+ e^{-\gamma z} + I_o^- e^{\gamma z} \tag{1.7b}$$

where the first and second terms correspond to wave propagation in $+z$ and $-z$ directions, respectively. By combining (1.3) and (1.7), it follows that the relation between voltage and current for the traveling waves, also known as the characteristic impedance, is given by

$$Z_o = \frac{V_o^+}{I_o^+} = \frac{-V_o^-}{I_o^-} = \sqrt{\frac{R' + j\omega L'}{G' + j\omega C'}} \tag{1.8}$$

For lossless lines, the voltage and current in the line are in phase, and the characteristic impedance is a real number:

$$Z_o = \sqrt{\frac{L'}{C'}} \tag{1.9}$$

Although losses may limit the performance of distributed microwave circuits, losses are usually neglected for design purposes, and the propagation constant and characteristic impedance are approximated by (1.6) and (1.9), respectively. According to (1.6), the dispersion relation β–ω is linear. The phase velocity, v_p, and the group velocity, v_g, are thus identical and given by

$$v_p = \frac{\omega}{\beta} = \frac{1}{\sqrt{L'C'}} \tag{1.10}$$

$$v_g = \left(\frac{d\beta}{d\omega}\right)^{-1} = \frac{1}{\sqrt{L'C'}} \tag{1.11}$$

and the wavelength in the line is given by:

$$\lambda = \frac{2\pi v_p}{\omega} = \frac{2\pi}{\beta} = \frac{2\pi}{\omega\sqrt{L'C'}} \tag{1.12}$$

That is, it is inversely proportional to frequency.[8] Sometimes, the length of a transmission line (for a certain frequency) is given in terms of the wavelength, or expressed as electrical length, $\phi = \beta l$, where l is the physical length of the line, and ϕ is an angle indicating whether distributed effects should be taken into account or not (as a first-order approximation, distributed effects are typically neglected if $\phi < \pi/4$). In many distributed circuits, transmission lines and stubs are $\lambda/4$ or $\lambda/2$ long at the operating frequency, corresponding to electrical lengths of $\phi = \pi/2$ and $\phi = \pi$, respectively.

For plane waves in source-free, linear, isotropic, homogeneous, and lossless dielectrics, the wave impedance, defined as the ratio between the electric and magnetic fields, and the phase velocity, are given by [1, 2] (see Appendix A):

$$\eta = \sqrt{\frac{\mu}{\varepsilon}} \tag{1.13}$$

[8] As will be shown, for artificial transmission lines expressions (1.10–1.12) are not necessarily valid. Indeed, for certain artificial lines, the wavelength either increases or decreases with frequency depending on the frequency regions.

$$v_p = \frac{1}{\sqrt{\mu\varepsilon}} \tag{1.14}$$

where ε and μ are the dielectric permittivity and magnetic permeability, respectively. These expressions, derived from Maxwell's equations, do also apply to TEM wave propagation in planar transmission lines, and therefore the main line parameters can be expressed in terms of the material parameters.[9] Notice that for nonmagnetic materials $\mu = \mu_o$, the permeability of vacuum, and hence the phase velocity can be rewritten in the usual form:

$$v_p = \frac{1}{\sqrt{\mu_o \varepsilon}} = \frac{1}{\sqrt{\mu_o \varepsilon_o \varepsilon_r}} = \frac{c}{\sqrt{\varepsilon_r}} \tag{1.15}$$

where c is the speed of light in vacuum, and $\varepsilon = \varepsilon_o \varepsilon_r$ (ε_o and ε_r being the permittivity of vacuum and the dielectric constant, respectively). However, for open nonhomogeneous lines, such as microstrip or coplanar waveguide (CPW) transmission lines, where pure TEM wave propagation is not possible, the previous expression does not hold. Nevertheless, the phase velocity in open lines can be expressed as (1.15) by simply replacing the dielectric constant of the substrate material, ε_r, with an effective dielectric constant, ε_{re}, which takes into account the presence of the electric field lines in both the substrate material and air[10]:

$$v_p = \frac{c}{\sqrt{\varepsilon_{re}}} \tag{1.16}$$

1.3 LOADED (TERMINATED) TRANSMISSION LINES

A uniform (in the direction of propagation) transmission line is characterized by the phase constant β (or by the electrical length βl), and by the characteristic impedance, Z_o. In a semi-infinitely long transmission line with a traveling wave generated by a source, the characteristic impedance expresses the relation between voltage and current at any transverse plane of the line. If losses are neglected, it follows that the power carried by the traveling wave along the line is given by

$$P^+ = \frac{1}{2}\frac{\left|V_o^+\right|^2}{Z_o} \tag{1.17}$$

[9] However, the wave impedance should not be confused with the characteristic impedance, Z_o, of transmission lines supporting TEM waves, which relates the voltage and current in the line and depends not only on the material parameters but also on the geometry of the line (see Appendix A).

[10] See at the end of Appendix A for more details.

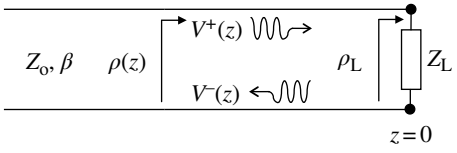

FIGURE 1.4 Transmission line terminated with an arbitrary load, located at $z = 0$.

However, if the line is terminated by a load, three different situations may arise: (1) the incident power is completely absorbed by the load, (2) the incident power is completely reflected by the load, and (3) the incident power is partially absorbed and reflected by the load. Let us consider that the impedance of the load is Z_L, that this load is situated in the plane $z = 0$ of the line (as Fig. 1.4 illustrates), and that a traveling wave of the form $V^+(z) = V_o^+ \cdot e^{-j\beta z}$ is present in the line. The ratio of voltage to current for such travelling wave is $V^+(z)/I^+(z) = Z_o$. At $z = 0$, the relation between the voltage, V_L, and the current, I_L, in the load must satisfy the Ohm law, that is, $V_L/I_L = Z_L$. Since, in general, $Z_L \neq Z_o$, a reflected wave must be generated at $z = 0$, so that the Ohm law is preserved. Therefore, the voltage and current in the line can be expressed as follows:

$$V(z) = V_o^+ e^{-j\beta z} + V_o^- e^{j\beta z} \tag{1.18a}$$

$$I(z) = \frac{V_o^+}{Z_o} e^{-j\beta z} - \frac{V_o^-}{Z_o} e^{j\beta z} \tag{1.18b}$$

By forcing the Ohm law at $z = 0$, it follows that

$$Z_L = \frac{V(0)}{I(0)} = \frac{V_o^+ + V_o^-}{V_o^+ - V_o^-} Z_o \tag{1.19}$$

and the relation between the amplitude of the reflected and the incident wave, also known as reflection coefficient, is

$$\rho_L = \frac{V_o^-}{V_o^+} = \frac{Z_L - Z_o}{Z_L + Z_o} \tag{1.20}$$

From (1.20), it follows that if $Z_L = Z_o$ (matched load), $\rho_L = 0$ and the incident power is absorbed by the load (i.e., there are not reflections in the load). Conversely, if the load is an open or a short circuit, the reflection coefficient is $\rho_L(Z_L = \infty) = 1$ and $\rho_L(Z_L = 0) = -1$, respectively, and the incident power is reflected back to the source. Notice that the incident power is also reflected back to the source for reactive loads, where $|\rho_L(Z_L = j\chi)| = 1$, χ being the reactance. Partially reflected and absorbed power

occurs for resistive loads not matched to the line, or for complex loads. Notice also that for passive loads ($Z_L = R + j\chi$, with $R > 0$), the modulus of the reflection coefficient is $|\rho_L| \leq 1$. This is expected since the reflected power, given by

$$P^- = \frac{1}{2}\frac{|V_o^+|^2}{Z_o}|\rho_L|^2 \tag{1.21}$$

cannot be higher than the incident power (given by 1.17) for passive loads. In microwave engineering, the reflection coefficient is typically expressed in dB and identified as the return loss:

$$RL = -20\log|\rho_L| \tag{1.22}$$

For infinitely long transmission lines or for transmission lines terminated with a matched load, constant amplitude travelling waves are present in the line. However, if a reflected wave is generated in the load plane, a standing wave is generated in the line, where the amplitude is modulated by the modulus of the reflection coefficient. From (1.18a) and (1.20), the voltage in the line can be written as follows:

$$V(z) = V_o^+\left[e^{-j\beta z} + \rho_L e^{j\beta z}\right] \tag{1.23}$$

If we now express the reflection coefficient in polar form ($\rho_L = |\rho_L| \cdot e^{j\theta}$), the voltage in the line can be rewritten as follows:

$$V(z) = V_o^+ e^{-j\beta z}\left[1 + |\rho_L| e^{2j\beta z + j\theta}\right] \tag{1.24}$$

from which it follows:

$$|V(z)|^2 = \left|V_o^+\right|^2\left[1 + |\rho_L|^2 + 2|\rho_L|\cos(2\beta z + \theta)\right] \tag{1.25}$$

Equation 1.25 indicates that the amplitude is a maximum ($V_{max} = |V_o^+|[1+|\rho_L|]$) and a minimum ($V_{min} = |V_o^+|[1-|\rho_L|]$) at planes separated by $\lambda/4$, and the ratio between the maximum and minimum voltage in the line, known as voltage standing wave ratio, is given by

$$\text{SWR} = \frac{1 + |\rho_L|}{1 - |\rho_L|} \tag{1.26}$$

As anticipated, the SWR is determined by the reflection coefficient. However, it only depends on the modulus of the reflection coefficient, not on its phase, θ. This means that from the information of the SWR, it is not possible to completely characterize the load. For instance, it is not possible to distinguish between a short circuit, an open circuit, or a reactive load, since the reflection coefficient of these loads has the same modulus ($|\rho_L| = 1$). Nonetheless, in many applications the relevant information is the

matching between the line (or the source) and the load in terms of the power transmitted to the load, the phase information being irrelevant.

Although wave reflection in a transmission line is caused by a mismatch between the line and the load, and hence it is ultimately generated at the plane of the load ($z = 0$), the reflection coefficient can be generalized to any plane of the line, as the ratio between the voltage of the incident and reflected wave, that is

$$\rho(z) = \frac{V^-}{V^+} = \frac{V_o^- e^{j\beta z}}{V_o^+ e^{-j\beta z}} = \rho_L e^{2j\beta z} \tag{1.27}$$

where, as expected, $|\rho(z)| = |\rho_L|$.

One important point of terminated lines is the amount of power delivered by a given source to the line. If the source has complex impedance, Z_s, such power is directly characterized by the power wave reflection coefficient, s, given by [9]:

$$s = \frac{Z_{in} - Z_s^*}{Z_{in} + Z_s} \tag{1.28}$$

where the asterisk denotes complex conjugate, and Z_{in} is the impedance seen from the input port of the line, that is, looking into the load (Fig. 1.5). Actually, the power transmission coefficient, which is the relevant parameter for computing the power transmitted to the line for the general situation of a source with complex impedance, is given by

$$\tau = 1 - |s|^2 = 1 - \left| \frac{Z_{in} - Z_s^*}{Z_{in} + Z_s} \right|^2 \tag{1.29}$$

The input impedance, Z_{in}, depends on the distance between the load and the input port (i.e., the plane of the source). This impedance can be simply computed as follows:

$$Z_{in} = \frac{V(-l)}{I(-l)} = \frac{V_o^+ \left(e^{j\beta l} + \rho_L e^{-j\beta l}\right)}{V_o^+ \left(e^{j\beta l} - \rho_L e^{-j\beta l}\right)} Z_o \tag{1.30}$$

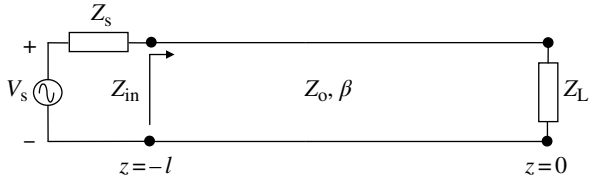

FIGURE 1.5 Transmission line of length l fed by a voltage source and terminated with an arbitrary load, located at $z = 0$.

And after some minor manipulation,

$$Z_{\text{in}} = Z_{\text{o}} \frac{Z_{\text{L}} + jZ_{\text{o}} \tan(\beta l)}{Z_{\text{o}} + jZ_{\text{L}} \tan(\beta l)} \tag{1.31}$$

The analysis of (1.31) reveals that in the limit $\beta l \to 0$, $Z_{\text{in}} = Z_{\text{L}}$, as expected, since this regime corresponds to the lumped element approximation discussed in Section 1.1. Expression (1.31) also indicates that the need to model the line as a distributed circuit does not solely depend on frequency (through β), but also on the line length l. Indeed, the key parameter is the electrical length, βl, as anticipated in the previous subsection. From (1.31), it follows that the input impedance is a periodic function with βl, and hence a periodic function with both the line length and the frequency. If the frequency is set to a certain value, the input impedance is a periodic function of period $\lambda/2$ with the line length. This means that the input impedance looking into the load seen from planes separated by a multiple of $\lambda/2$ is identical. From this result, it follows that for a $\lambda/2$ line ($\beta l = \pi$), the input impedance is the one of the load, $Z_{\text{in}} = Z_{\text{L}}$.

Let us now consider several cases of particular interest. If the line length is $l = \lambda/4$ ($\beta l = \pi/2$), the input impedance is

$$Z_{\text{in}} = \frac{Z_{\text{o}}^2}{Z_{\text{L}}} \tag{1.32}$$

which means that the input impedance is inversely proportional to the load impedance, and hence a $\lambda/4$ transmission line acts as an impedance inverter. This means that a reactive load with inductive/capacitive reactance is seen as capacitive/inductive reactance from the input port; in other words, the sign of the reactance is reversed in $\lambda/4$ lines. From (1.32), it also follows that an open-circuit load is transformed to short-circuit at the input port of a $\lambda/4$ line, and vice versa.

For the general case of open-ended ($Z_{\text{L}} = \infty$) and short-circuited ($Z_{\text{L}} = 0$) lines, the input impedance given by (1.31) takes the following form:

$$Z_{\text{in}}(Z_{\text{L}} = \infty) = -jZ_{\text{o}} \cot(\beta l) \tag{1.33a}$$

$$Z_{\text{in}}(Z_{\text{L}} = 0) = jZ_{\text{o}} \tan(\beta l) \tag{1.33b}$$

Thus, the input impedances are purely reactive, just as those of lumped reactive elements (inductors and capacitors). For lines satisfying $\beta l < \pi/2$, a short-circuited line resembles an inductor, whereas an open-ended line mimics a capacitor. However, the reactances of lumped inductors and capacitors have different mathematical forms than those of shorted and opened transmission lines. This means that we cannot replace lumped reactive elements with open or shorted lines exhibiting identical behavior. However, by forcing the impedance of a capacitor and inductor to be equal to those of (1.33) we obtain

$$-\frac{j}{\omega C} = -jZ_o \cot(\beta l) \tag{1.34a}$$

$$j\omega L = jZ_o \tan(\beta l) \tag{1.34b}$$

and the previous expressions have solutions at many different frequencies. Let us consider the smallest of these angular frequencies and call it ω_c. If we set the length of the line to be $\lambda/8$ at this frequency (i.e., $\beta l = \pi/4$ at ω_c), the previous expressions take the following form:

$$\frac{1}{\omega_c C} = Z_o \tag{1.35a}$$

$$\omega_c L = Z_o \tag{1.35b}$$

Therefore, if we wish to implement a short-circuited transmission line with the same impedance as an inductor L at frequency ω_c, we set the characteristic impedance of the transmission line to $Z_o = \omega_c L$. Likewise, if we wish to obtain the reactance of a capacitor C at frequency ω_c, we set the characteristic impedance of the transmission line to $Z_o = 1/\omega_c C$. In both cases, the length of the line must be set to $\lambda/8$ at ω_c. Expressions (1.35) are called Richard's transformations [10], and are useful to avoid the use of lumped reactive components in certain microwave circuits such as low-pass filters. However, since Richard's transformations guarantee identical reactances between the lumped and the distributed reactive elements at a single frequency, we cannot expect that the response of a lumped circuit is identical to that of the distributed counterpart.

Obviously, the load of a transmission line can be another transmission line with different characteristic impedance. Let us consider that two transmission lines of characteristic impedances Z_o and Z_1, respectively, are cascaded as shown in Figure 1.6, and that the transmission line to the right of the contact plane ($z = 0$), that is, the line acting as load, is either infinitely long or terminated with a matched load (so that there are not reflected waves in this line). Under these conditions, the load impedance seen by the transmission line to the left of $z = 0$ is simply Z_1. Hence, the reflection coefficient at $z = 0$ is given by

$$\rho = \frac{Z_1 - Z_o}{Z_1 + Z_o} \tag{1.36}$$

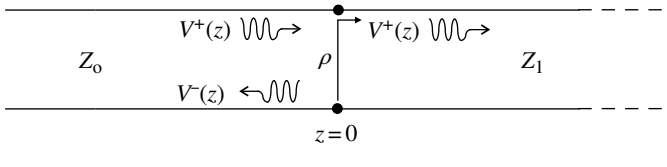

FIGURE 1.6 Cascade connection of two transmission lines with different characteristic impedance.

and the incident wave is partially transmitted to the second line. For $z < 0$, the voltage in the line can be expressed as (1.23), whereas to the right of the contact plane, the voltage can be expressed in terms of a transmission coefficient, T, as follows:

$$V(z) = V_o^+ T e^{-j\beta z} \tag{1.37}$$

By forcing expressions (1.23) and (1.37) to be identical at $z = 0$, the transmission coefficient is found to be

$$T = 1 + \rho = \frac{2Z_1}{Z_1 + Z_o} \tag{1.38}$$

and the transmission coefficient expressed in dB is identified as the insertion loss:

$$IL = -20\log|T| \tag{1.39}$$

Notice that the transmission coefficient, defined by the fraction of the amplitude of the voltage of the incident wave transmitted to the second transmission line (expression 1.37), can be higher than one (this occurs if $Z_1 > Z_o$). This result does not contradict any fundamental principle (i.e., the conservation of energy), since the transmitted power is always equal or less than the incident power (however, the amplitude of the voltage of the transmitted wave can be higher than V_o^+).

To end this subsection, let us briefly consider the reflections generated by a source with mismatched impedance that feeds a transmission line with characteristic impedance Z_o and length l (Fig. 1.5). Let us assume that the load of the transmission line is also mismatched, so that a reflected wave is generated by the load once the incident wave reaches the load plane. Once the switch is closed at $t = 0$, the following expression must be satisfied at any time $t > 0$:

$$V_s = Z_s I(-l) + V(-l) \tag{1.40}$$

Before the reflected wave at the load reaches the plane of the source ($z = -l$), that is, for $t < 2l/v_p$, expression (1.40) is written as follows:

$$V_s = Z_s \frac{V_1^+}{Z_o} + V_1^+ \tag{1.41}$$

where V_1^+ is the amplitude of the incident wave generated by the source after the switch is closed, that is,[11]

[11] This expression is valid if the source impedance is purely resistive. However, expression (1.45) is valid for any source impedance (purely resistive, purely reactive, or complex). The reason is that the time domain analysis giving (1.45) can be initiated once the transient associated to reactive or complex load and/or source impedances has expired.

$$V_1^+ = V_s \frac{Z_o}{Z_o + Z_s} \tag{1.42}$$

Once the reflected wave V_1^- reaches the source plane, a reflected wave V_2^+ must be generated by the source in order to satisfy the Ohm law. Hence, (1.40) is expressed as follows:

$$V_s = Z_s \frac{V_1^+ - V_1^- + V_2^+}{Z_o} + V_1^+ + V_1^- + V_2^+ \tag{1.43}$$

By combining (1.41) and (1.43), we obtain the following:

$$\frac{Z_s}{Z_o}\left(V_1^- - V_2^+\right) = V_1^- + V_2^+ \tag{1.44}$$

and the reflection coefficient at the source is found to be

$$\rho_s = \frac{V_2^+}{V_1^-} = \frac{Z_s - Z_o}{Z_s + Z_o} \tag{1.45}$$

which is formally identical to the reflection coefficient at the load.

Obviously, when the reflected wave at the source (V_2^+) reaches the load plane, a new wave (V_2^-) is generated by reflection at the load plane, and the process continues indefinitely until the steady state is achieved. This endless bouncing process converges to a steady state since the amplitude of the reflected waves progressively decreases.[12] Let us calculate, as an illustrative example, the steady-state voltage at $z = -l$ for the structure of Figure 1.5. If the initial wave is designated as V_1^+, the first reflected one at $z = -l$, taking into account the phase shift experienced by the wave along the transmission line, is $V_1^- = V_1^+ \rho_L \cdot e^{-2j\beta l}$ (see Fig. 1.7). The next two are $V_2^+ = V_1^+ \rho_L \rho_s \cdot e^{-2j\beta l}$ and $V_2^- = V_1^+ \rho_L^2 \rho_s \cdot e^{-4j\beta l}$. The steady-state voltage at $z = -l$ is given by the superposition of the left to right (+) and right to left (−) waves, that is[13],

$$V(z = -l) = \sum_i V_i^+ + \sum_i V_i^- = V_1^+ \frac{1}{1 - \rho_i \rho_s} + V_1^+ \frac{\rho_i}{1 - \rho_i \rho_s} \tag{1.46}$$

where V_1^+ is given by (1.42) and $\rho_i = \rho_L \cdot e^{-2j\beta l}$. Introducing (1.42) and (1.45) in (1.46) gives

$$V(z = -l) = V_s \frac{Z_o\left(1 + \rho_L e^{-2j\beta l}\right)}{Z_o + Z_s - (Z_s - Z_o)\rho_L e^{-2j\beta l}} \tag{1.47}$$

[12] This is consequence of the modulus of the reflection coefficients at the source and the load, which is smaller than one for passive loads. However, if the line is loaded with an active load, instability is potentially possible.

[13] To derive (1.46), the identity $1 + x + x^2 + \ldots = 1/(1 - x)$, where $|x| < 1$, has been used.

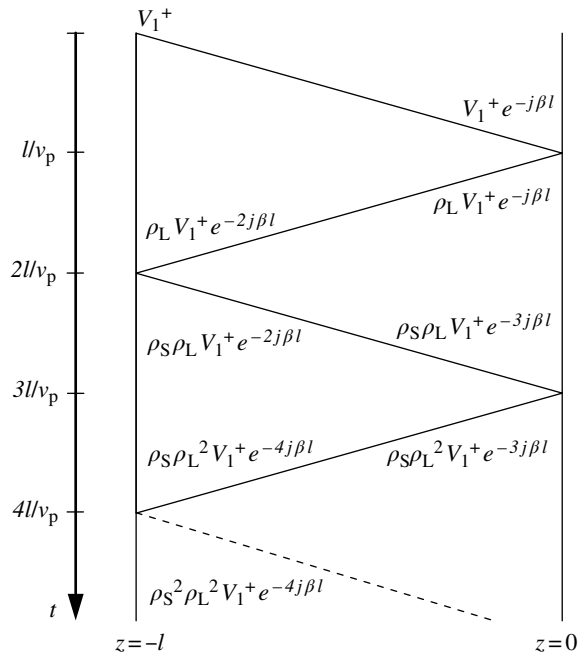

FIGURE 1.7 Bounce diagram corresponding to the example discussed in the text. The vertical axis is the time axis.

which can be expressed as follows:

$$V(z=-l) = V_s \frac{Z_{in}}{Z_{in} + Z_s} \tag{1.48}$$

where Z_{in}, given by (1.30), is the impedance seen from the source plane. As expected, the steady-state voltage at $z=-l$ is simply given by the voltage divider, considering the series connection of the source impedance and the input impedance of the loaded line.

1.4 LOSSY TRANSMISSION LINES

In planar transmission lines of practical interest for RF and microwave circuit design losses are small and they are usually neglected for design purposes (as it was mentioned in Section 1.2).[14] However, although small, losses produce

[14] To guarantee small losses, distributed circuits must be preferably implemented in commercially available low-loss microwave substrates.

attenuation and distortion in the transmitted signals, and the analysis of their effects on wave propagation is of interest. There are three main causes of losses: (1) the finite conductivity of the metals (conductor losses), (2) the dissipation in the dielectric (either caused by the presence of free electrons or by dipole relaxation phenomena), and (3) radiation losses. Although radiation losses may be dominant under some circumstances, transmission lines operating as guided-wave structures must be designed in order to exhibit small radiation. Hence, this loss mechanism is not considered by the moment.[15]

Ohmic (or conductor) and dielectric losses are accounted for by the lumped element circuit model of the transmission line (Fig. 1.3) through the series resistance R' and shunt conductance G', respectively. Let us now calculate the complex propagation constant (expression 1.5) under the low-loss approximation (justified by the reasons explained earlier), namely, $R' \ll \omega L'$ and $G' \ll \omega C'$. The complex propagation constant can be rearranged and written as follows:

$$\gamma = j\omega\sqrt{L'C'}\sqrt{1 - j\left(\frac{R'}{\omega L'} + \frac{G'}{\omega C'}\right) - \frac{R'G'}{\omega^2 L'C'}} \tag{1.49}$$

Neglecting the last term in the square root of (1.49) and applying the Taylor series expansion up to the first order, the complex propagation constant can be approximated by

$$\gamma = j\omega\sqrt{L'C'}\left[1 - \frac{j}{2}\left(\frac{R'}{\omega L'} + \frac{G'}{\omega C'}\right)\right] \tag{1.50}$$

From (1.50), the attenuation constant and the phase constant for low-loss transmission lines can be easily identified:

$$\alpha = \frac{1}{2}\left(\frac{R'}{Z_o} + G'Z_o\right) \tag{1.51}$$

$$\beta = \omega\sqrt{L'C'} \tag{1.52}$$

where Z_o is the lossless characteristic impedance of the line given by (1.9).

[15] Nevertheless, leaky-wave transmission lines are specifically designed to enhance radiation. These lines are the building blocks of leaky-wave antennas (LWAs), as will be shown in Chapter 4.

With regard to the characteristic impedance (expression 1.8), it can be rearranged and written as follows:

$$Z_o = \sqrt{\frac{L'}{C'}} \sqrt{1 - j\frac{\dfrac{C'\omega}{G'} - \dfrac{L'\omega}{R'}}{\dfrac{L'C'\omega^2}{R'G'} - j\dfrac{L'\omega}{R'}}} \tag{1.53}$$

By virtue of the low-loss approximation, the second term of the denominator in the square root can be neglected, and, by using the first order Taylor series approximation, the characteristic impedance is found to be

$$Z_o = \sqrt{\frac{L'}{C'}}\left[1 - \frac{j}{2}\left(\frac{R'}{\omega L'} - \frac{G'}{\omega C'}\right)\right] \tag{1.54}$$

and this expression can be further simplified to (1.9).[16]

According to these results, it follows that the phase constant and the characteristic impedance of low-loss transmission lines can be closely approximated by considering the line as lossless. The attenuation constant (1.51) has two contributions: one associated to conductor losses (proportional to R'), and one associated to dielectric losses (proportional to G').

Despite for low-loss lines the phase constant can be approximated by a linear function, the effects of dispersion may be appreciable in very long transmission lines, and may give rise to signal distortion. However, there is a special case where the phase constant of lossy transmission lines varies linearly with frequency, and dispersion is not present. Such lines are called distortionless lines and must satisfy the following identity (known as distortionless, or Heaviside, condition)

$$R'C' = G'L' \tag{1.55}$$

In view of the general expression of the complex propagation constant (1.5), the unique way to achieve a linear dependence of β with frequency for a lossy line is to achieve a complex propagation constant of the form $A + j\omega B$ (where A and B are constants). The only way this can be satisfied is if $R' + j\omega L'$ and $G' + j\omega C'$ differ by no more than a constant factor. This means that both the real and imaginary parts must be independently related by the same factor, which leads to (1.55). Under the condition specified by (1.55), the complex propagation constant is[17]

$$\gamma = \frac{R'}{Z_o} + j\omega\sqrt{L'C'} \tag{1.56}$$

[16] Notice that this means to neglect $R'/\omega L'$ and $G'/\omega C'$ in (1.54). However, if these two terms are neglected in (1.50), we find the trivial solution corresponding to the lossless line, with β given by (1.6) and $\alpha = 0$.

[17] Notice that, using (1.55), the attenuation constant can also be expressed as $\alpha = (R'G')^{1/2}$ or $\alpha = G'Z_o$.

and β is given by (1.6). It is interesting to mention that the attenuation constant ($\alpha = R'/Z_o$) does not depend on frequency, which means that all frequency components are attenuated the same factor. This means that distortionless lines are able to transmit pulse signals or modulated signals without distortion (although these signals are attenuated along the line due to losses). It is also simply to demonstrate that the characteristic impedance of distortionless lines is a real constant given by (1.9).

In practical transmission lines, the distortionless condition is not easy to satisfy since G' is usually very small. To compensate this, the line can be loaded with series connected inductances periodically spaced along the line. This strategy leads to an unconventional transmission line that can indeed be considered an artificial transmission line.[18] Nevertheless, the elements of the distributed circuit of a transmission line are not exactly constant (in particular, R' varies weakly with frequency), and the distortionless condition (expression 1.55) is difficult to meet in practice. For planar transmission lines used as building blocks in distributed circuits, where the lines are low-loss and short, dispersion is not usually an issue, except at high frequencies (dozens of GHz) or for very wideband signals.

1.4.1 Dielectric Losses: The Loss Tangent

Although for the design of most planar distributed circuits losses are neglected in the first steps, it is important to simulate their effects before fabrication. In EM solvers, losses are introduced by providing the conductivity of the metallic layers, and the loss tangent ($\tan\delta$) of the substrate material. The loss tangent takes into account dielectric losses, including both conduction losses (due to nonzero conductivity of the material) and losses due to damping of the dipole moments (that represents an energy transfer between the external electric field and the material at microscopic level).

For a dielectric material, the application of an electric field gives rise to the polarization of the atoms or molecules of the medium in the form of electric dipole moments, which contribute to the total displacement flux according to

$$\vec{D} = \varepsilon_o \vec{E} + \vec{P}_e \tag{1.57}$$

where $\vec{P}_e$ is the electric polarization, which is related to the applied electric field through[19]

$$\vec{P}_e = \varepsilon_o \chi_e \vec{E} \tag{1.58}$$

[18] According to the definition of artificial transmission line adopted in this book (see Section 1.1), L-loaded distortionless lines belong to this group, but such lines are out of the scope of this manuscript. As will be seen in Chapter 2, periodic loaded lines exhibit a cut-off frequency. Beyond this frequency, attenuation dramatically increases, and hence these lines may not support the transmission of high-frequency or broadband signals.

[19] It is assumed that the material is linear, isotropic, and homogeneous, that is, the electric susceptibility and permittivity are scalars that do not depend on the position and magnitude of the external field. For anisotropic materials, the relation between $\vec{E}$ and $\vec{P}_e$, or between $\vec{E}$ and $\vec{D}$, is a tensor.

χ_e being the electric susceptibility. Combining the previous expressions, the electric displacement can be written as follows:

$$\vec{D} = \varepsilon_o(1+\chi_e)\vec{E} = \varepsilon\vec{E} \tag{1.59}$$

In vacuum, the electric susceptibility is null, whereas in dielectric materials it is a complex number, where the imaginary part accounts for losses. In low-loss materials, the imaginary part of the susceptibility can be neglected to a first-order approximation. However, the effects of material losses on circuit performance may play a role in distributed circuits.[20] For this reason, losses cannot be neglected in the evaluation of circuit performance (typically inferred from commercially available EM simulators). In lossy materials, the dielectric permittivity is thus a complex number that can be expressed as follows:

$$\varepsilon = \varepsilon_o(1+\chi_e) = \varepsilon' - j\varepsilon'' \tag{1.60}$$

where ε'' is a positive number due to energy conservation [1, 11].

Conduction losses, associated to the presence of free electrons in the dielectric material (it is assumed that the material exhibits a nonzero conductivity), do also contribute to the imaginary part of the complex permittivity. The conduction current density is related to the electric field through the Ohm law:

$$\vec{J} = \sigma\vec{E} \tag{1.61}$$

where σ is the conductivity of the material. By introducing the previous expression in the Ampere–Maxwell law, we obtain

$$\nabla\times\vec{H} = j\omega\varepsilon\vec{E} + \sigma\vec{E} \tag{1.62a}$$

$$\nabla\times\vec{H} = j\omega\left(\varepsilon' - j\frac{\sigma+\omega\varepsilon''}{\omega}\right)\vec{E} \tag{1.62b}$$

From (1.62), it is clear that the effects of conduction losses can be accounted for by including a conductivity dependent term in the imaginary part of the complex permittivity. The loss tangent is defined as the ratio between the imaginary and real parts of this generalized[21] permittivity:

[20] In low-loss microwave substrates, losses are dominated by the finite conductivity of the metal layers. However, in general-purpose substrates, such as FR4, or in high-resistivity silicon (HR-Si) substrates, among others, material losses may significantly degrade the circuit performance.

[21] The complex permittivity including the contribution of σ is usually designated as effective complex permittivity in most textbooks. However, in this book, the term *effective permittivity* is either referred to the permittivity of effective media, or metamaterials, as will be seen in Chapter 3, or it is used to describe wave propagation in quasi-TEM lines by introducing an "averaged" permittivity (and permeability) in the equations governing purely TEM wave propagation (see Appendix A).

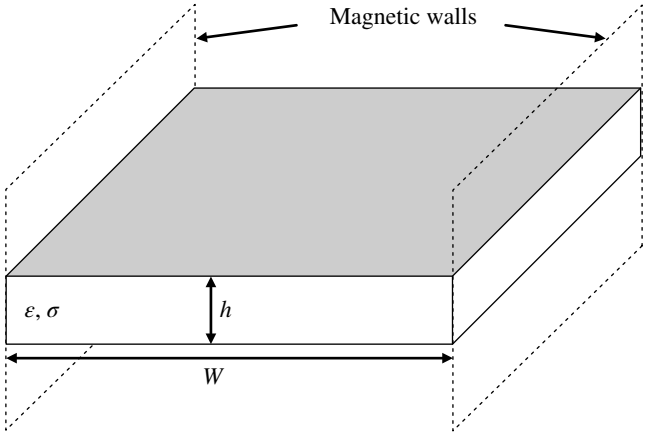

FIGURE 1.8 Parallel plate transmission line with magnetic walls at the edges.

$$\tan\delta = \frac{\sigma + \omega\varepsilon''}{\omega\varepsilon'} \tag{1.63}$$

Low-loss dielectrics are characterized by a small $\tan\delta$ (typically $10^{-4} - 10^{-2}$).

Let us now try to link the loss tangent to the dielectric contribution of the attenuation constant for low-loss transmission lines. Let us consider a hypothetical transmission line with purely TEM wave propagation, for example, a stripline, or a parallel plate transmission line with magnetic walls at the lateral sides (or with very wide plates to neglect the fringing fields). This simplifies the analysis, and provides compact formulas, which is enough for our purposes. For the case of the parallel plate transmission line (Fig. 1.8), let W and h be the width of the metal plates and the height of the substrate, respectively. The per-unit-length line conductance is related to the dielectric conductivity as[22]

$$G' = \frac{W}{h}\sigma \tag{1.64}$$

which in turn can be expressed in terms of the per unit length capacitance as

$$G' = \frac{C'}{\varepsilon'}\sigma \tag{1.65}$$

[22] We assume that the conductivity in (1.64) is actually the effective conductivity, given by the numerator of (1.63).

The dielectric contribution of the attenuation constant for low-loss lines is given by the second term of the right-hand side of (1.51), and can be written as follows:

$$\alpha_d = \frac{1}{2} G' \sqrt{\frac{L'}{C'}} \tag{1.66}$$

Introducing (1.65) in (1.66), we finally obtain

$$\alpha_d = \frac{1}{2}\frac{C'}{\varepsilon'}\sigma\sqrt{\frac{L'}{C'}} = \frac{1}{2}\frac{\sigma}{\varepsilon'}\frac{\beta}{\omega} = \frac{\beta}{2}\tan\delta = \frac{1}{2}\omega\sqrt{\mu\varepsilon'}\tan\delta \tag{1.67}$$

In nonhomogeneous open lines, such as microstrip lines or CPWs, expression (1.67) is not strictly valid, but it provides a rough approximation of α_d by merely introducing the effective permittivity (defined as the effective dielectric constant times the permittivity of vacuum) in the last term. Indeed, for microstrip transmission lines (1.67) rewrites as [12, 13] follows:

$$\alpha_d = \frac{\pi f}{c}\frac{\varepsilon_r(\varepsilon_{re}-1)}{\sqrt{\varepsilon_{re}}(\varepsilon_r-1)}\tan\delta \tag{1.68}$$

where it has been assumed that $\mu = \mu_o$ and $(\mu_o\varepsilon_o)^{-1}$ is the speed of light in vacuum, c. Notice that if $\varepsilon_r = \varepsilon_{re}$, (1.67) and (1.68) are identical. The analysis of (1.68) also reveals that for high values of ε_r (and hence ε_{re}), expression (1.67) provides a good estimation of α_d by introducing in the root the effective permittivity.

The dielectric material (substrate) used in planar transmission lines is characterized by the loss tangent (which accounts for dielectric losses) and by the dielectric constant (which determines the phase velocity). Although these parameters are supplied by the manufacturer with the corresponding tolerances, there are sometimes substantial variations that make necessary the characterization of the material (i.e., the measurement of the dielectric constant and the loss tangent) for an accurate design. The dielectric constant and the loss tangent of a substrate material can be experimentally inferred by means of a microstrip ring resonator configuration (Fig. 1.9) [13–15]. The transmission coefficient exhibits transmission peaks at frequencies that depend on the dielectric constant of the substrate, and the loss tangent is extracted from the quality factor of the resonance peaks along with the theoretical calculations of the conductor losses (see next subsection).

For a ring resonator, resonances occur at those frequencies where the ring circumference is a multiple of the wavelength, λ. The resonance condition can thus be expressed as follows:

$$\lambda = \frac{2\pi r_m}{n} = \frac{v_p}{f_n} = \frac{c}{\sqrt{\varepsilon_{re}}}\frac{1}{f_n} \tag{1.69}$$

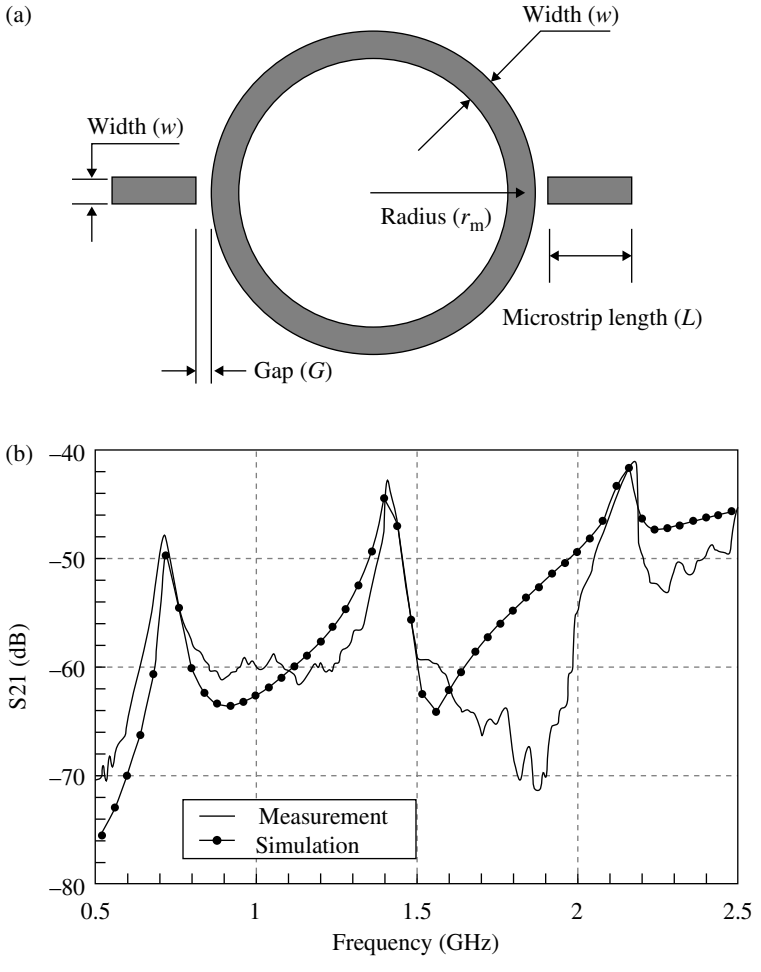

FIGURE 1.9 Microstrip ring resonator configuration used to extract the dielectric constant and loss tangent of the substrate (a), and typical frequency response with transmission peaks (b). Reprinted with permission from Ref. [15]; copyright 2007 IEEE.

where n refers to the nth-order resonance, and r_m is the mean ring radius. The effective dielectric constant is thus [13–15]

$$\varepsilon_{re} = \left(\frac{nc}{2\pi r_m f_n}\right)^2 \tag{1.70}$$

Once the effective dielectric constant is known (the resonance frequencies can be easily inferred from the measured transmission coefficient), the dielectric constant is given by [6, 13]:

$$\varepsilon_r = \frac{2\varepsilon_{re} + M - 1}{M + 1} \tag{1.71}$$

where

$$M = \left(1 + 12\frac{h}{W'}\right)^{-1/2} \tag{1.72}$$

and W' is the effective strip width, given by

$$W' = W + \frac{1.25t}{\pi}\left(1 + \ln\frac{2h}{t}\right) \tag{1.73}$$

In (1.72) and (1.73), h and t are the thickness of the substrate and metal layer, respectively, and W is the strip width. Expressions (1.71–1.73) are valid under the assumption that $W \geq h \gg t$, which is usually satisfied (general expressions are given in [6]).

For the determination of tanδ, it is first necessary to measure the unloaded quality factor, given by [13, 14]:

$$Q_o = \frac{Q_L}{1 - 10^{-IL/20}} \tag{1.74}$$

where IL is the measured insertion loss at resonance, and the loaded quality factor is given by

$$Q_L = \frac{f_o}{BW_{-3\ dB}} \tag{1.75}$$

$BW_{-3\ dB}$ being the −3 dB bandwidth, which can be easily measured from the transmission coefficient. The total attenuation in the resonator is related to the unloaded quality factor by

$$\alpha = \frac{\pi}{Q_o \lambda} \tag{1.76}$$

where λ is given by (1.69). By subtracting to (1.76) the conduction attenuation constant, given by expression (1.90) (see the next subsection), the dielectric attenuation constant, α_d, can be inferred,[23] and by using (1.68), the loss tangent can be finally obtained.

[23] It is assumed that radiation from the ring is negligible (valid at moderate frequencies) [13]; hence, the contribution of radiation loss to the attenuation constant is null.

Alternatively, the dielectric constant and the loss tangent of thin film un-clad substrates and low-loss sheet materials can be measured by means of specific instrumentation, namely, a split cylinder resonator. It is a cylindrical resonant cavity separated into two halves, one of them being movable in order to accommodate varying sample thicknesses (i.e., the sample is loaded in the gap between the two cylinder halves). Each cylinder half accommodates a small coupling loop, introduced through a small hole, in order to measure the transmission coefficient of the fundamental TE_{011} mode. The principle for the determination of the dielectric constant and the loss tangent is the variation of the resonance frequency and quality factor with loaded and un-loaded cylinder (obviously, the thickness of the sample must be accurately known for a correct measurement). More details on this method are given in Refs. [16, 17].

1.4.2 Conductor Losses: The Skin Depth

Let us consider a conductor material with finite, but high, conductivity (i.e., a low-loss conductor), where the conduction current dominates over the displacement current, or $\sigma \gg |\omega\varepsilon'|, |\omega\varepsilon''|$. The complex propagation constant in such medium, with general expression given by (see Appendix A)

$$\gamma = \alpha + j\beta = j\omega\sqrt{\mu\left(\varepsilon' - j\frac{\sigma + \omega\varepsilon''}{\omega}\right)} \tag{1.77}$$

can be written as follows:

$$\gamma = j\omega\sqrt{\mu\left(-j\frac{\sigma}{\omega}\right)} = \frac{1+j}{\delta_p} \tag{1.78}$$

with

$$\delta_p = \sqrt{\frac{2}{\omega\mu\sigma}} \tag{1.79}$$

From (1.78), it follows that both the phase constant and the attenuation constant are given by

$$\alpha = \beta = \frac{1}{\delta_p} \tag{1.80}$$

Since the attenuation of the fields is given by $e^{-\alpha z} = e^{-z/\delta p}$, where z is the direction of propagation, δ_p indicates the distance over which a plane wave is attenuated by a factor of e^{-1}. If a plane wave in vacuum impinges on a conductor material with its surface perpendicular to the wave vector, the wave transmitted to the conductor decays

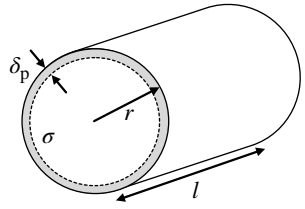

FIGURE 1.10 Cylindrical conductor with conductivity σ. The effective cross section for the calculation of the AC resistance is given by the annular gray region corresponding to one skin depth.

exponentially from its surface. Therefore, δ_p is referred to as penetration depth.[24] It is worth mentioning that (i) δ_p decreases with the square root of the conductivity and frequency, and (ii) the wavelength is given by $\lambda = 2\pi\delta_p$ and is typically much smaller than the wavelength in free space.

Similarly, if a conductor such as a wire or a metallic strip is carrying an AC current, the current tends to concentrate in the conductor surface as frequency increases. This phenomenon is known as *skin effect* and increases the high frequency AC resistance of the conductor since the effective conductor cross section is reduced. To a first-order approximation, the effective cross section of the conductor is limited by the external surface contour and by the curve resulting by reducing such contour by the penetration depth, also known as skin depth. Let us consider as a simple illustrative example a cylindrical conductor with length l and radius r (Fig. 1.10). The AC resistance is given by

$$R_{AC} = \frac{l}{\sigma A_{AC}} = \frac{l}{\sigma 2\pi r \delta_p} \tag{1.81}$$

where A_{AC} is the effective conductor cross section.

Expression (1.81) can also be derived by considering the intrinsic impedance of the low-loss conductor, given by[25]

$$\eta = \sqrt{\frac{\mu}{\varepsilon}} = \sqrt{j\frac{\mu}{\sigma}\omega} = (1+j)R_s \tag{1.82}$$

where R_s is the surface resistance

$$R_s = \frac{1}{\sigma\delta_p} = \sqrt{\frac{\mu\omega}{2\sigma}} \tag{1.83}$$

[24] In copper, the most used clad metal for PCB technology, the penetration depth (or skin depth) at 1 and 10 GHz is 2.06 and 0.66 μm, respectively.

[25] Notice that in a good conductor, the phase of the magnetic component of an EM wave propagating through it lags that of the electric component by π/4.

Considering again a plane wave impinging on the surface of a low-loss conductor, the conduction current density within the conductor is given by[26]

$$\vec{J} = \sigma \vec{E} = \sigma E_{\mathrm{o}} e^{-\frac{z}{\delta_{\mathrm{p}}}} \cdot e^{-j\frac{z}{\delta_{\mathrm{p}}}} \vec{x} \tag{1.84}$$

where E_{o} is the electric field in the surface, and it has been assumed that the electric field is polarized in the x-direction. The current across a surface normal to $\vec{x}$, of width a and infinitely long in the direction normal to the surface (z-direction) is given by:

$$I = \int_0^{\infty} dz \int_{y_{\mathrm{o}}}^{y_{\mathrm{o}}+a} dy \left(\sigma E_{\mathrm{o}} e^{-\frac{z}{\delta_{\mathrm{p}}}} \cdot e^{-j\frac{z}{\delta_{\mathrm{p}}}} \right) \tag{1.85}$$

which gives

$$I = a\sigma E_{\mathrm{o}} \frac{\delta_{\mathrm{p}}}{1+j} = \frac{aE_{\mathrm{o}}}{R_{\mathrm{s}}(1+j)} \tag{1.86}$$

The voltage drop between two points separated a distance l in the x-direction is simply $V = E_{\mathrm{o}} l$. Thus, the surface impedance is given by

$$Z_{\mathrm{s}} = R_{\mathrm{s}}(1+j)\frac{l}{a} \tag{1.87}$$

which reduces $R_{\mathrm{s}}(1+j)$ for a square geometry. The term R_{s} is usually designated as square resistance. For the cylindrical conductor considered earlier, the AC resistance can thus be inferred from the real part of (1.87) by considering $a = 2\pi r$, which gives (1.81).

Deriving the relation between the conduction loss attenuation constant, α_{c}, and the surface (or square) resistance in most planar transmission lines is not straightforward. Nevertheless, for a parallel plate transmission line, the per-unit-length resistance is roughly given by [12]

$$R' = \frac{2R_{\mathrm{s}}}{W} \tag{1.88}$$

where W is the width of the strips. The previous expression is valid under the assumption that the current density is uniform in the transverse plane and concentrated one

[26] This result is also obtained from Maxwell's equations by calculating the current density distribution in the direction normal to the surface (z-direction) of a semi-infinite conductor, with current density parallel to such surface, and assuming that the current density at the surface is $J_x\ (z=0) = \sigma E_{\mathrm{o}}$ (see Appendix D).

skin depth from the interface between the conductors and the substrate. Introducing (1.88) in the first term of (1.51), gives

$$\alpha_c = \frac{R_s}{Z_o W} \tag{1.89}$$

For microstrip lines, closed-form expressions for α_c have been derived in [12]. Specifically, if $W \geq 2h$[27]

$$\alpha_c = \frac{R_s}{Z_o h} \frac{1}{\left\{ \frac{W'}{h} + \frac{2}{\pi} \ln\left[2\pi e \left(\frac{W'}{2h} + 0.94 \right) \right] \right\}^2} \cdot \left[\frac{W'}{h} + \frac{W'/\pi h}{\frac{W'}{2h} + 0.94} \right] \times \left\{ 1 + \frac{h}{W'} + \frac{h}{\pi W'} \left[\ln\left(\frac{2h}{t} + 1 \right) - \frac{1 + t/h}{1 + t/2h} \right] \right\} \tag{1.90}$$

The conduction attenuation constants for microstrip lines satisfying $W/h \leq 1/2\pi$ and $1/2\pi < W/h \leq 2$ are reported in Ref. [12]. It is worth mentioning that (1.90) simplifies to (1.89) in the limit of wide strips ($W/h \gg 1$).

1.5 COMPARATIVE ANALYSIS OF PLANAR TRANSMISSION LINES

The objective of this subsection is to briefly highlight some advantages and limitations of planar transmission lines from a comparative viewpoint. The most used transmission lines for the implementation of planar distributed circuits are microstrip lines and CPWs because no more than two metal levels are needed for their implementation. Striplines are closed and shielded structures, but they require three metal levels and their use is very limited. However, striplines support TEM wave propagation, and the phase velocity in these lines does not depend on their lateral geometry (i.e., the strip width).[28] Conversely, microstrip lines and CPWs are nonhomogeneous open lines that do not support purely TEM waves, but quasi-TEM waves. The dielectric substrate slows the waves down, as compared to the field lines in air, and the field lines tend to bend forward, thus preventing the presence of TEM modes.

[27] If surface roughness is not negligible, its effects can be accounted for in (1.90) by merely including an additional term in R_s, as reported in [13]. In [12], α_c appears multiplied by the factor 8.68 since the units are given in dB/unit length. This factor arises from the conversion from Nepers (Np) to dB. The Neper is a unit in logarithmic scale that uses the natural logarithm. Thus, if an arbitrary variable $F(z)$ is attenuated with position as $F(z) = F_o \cdot \exp(-\alpha z)$, the loss factor expressed in Np is $-\ln[F(z)/F_o] = \alpha z$, and α is said to have units of Np/unit length. The loss factor expressed in dB is $-20\log[F(z)/F_o] = -20\log[\exp(-\alpha z)] = \alpha z 20\log(e) = 8.68\,\alpha z$. Hence, the conversion from Np/unit length to dB/unit length introduces the above number 8.68 in expression (1.90).

[28] For TEM wave propagation in a stripline, the substrate material must be homogeneous and isotropic. Strictly speaking, purely TEM waves do also require perfect conductors. This latter condition cannot be satisfied in practice, but as long as the resistivity of the conductors is low, purely TEM wave propagation can be assumed.

From the viewpoint of shielding, the advantage of microstrip lines over CPWs is the presence of the ground plane in the back substrate side, which effectively isolates the structure from the backside region, and prevents it from potential interference effects caused by other circuits or materials (including metallic holders). CPWs with backside metallization (also known as conductor-backed CPWs) can also be implemented, but this backside metallization may induce leaky wave propagation as a result of the parasitic parallel plate waveguides present at both sides of the CPW axis. As compared to microstrip lines, CPWs without backside ground plane only need a metallic layer for their implementation. This eases fabrication and the shunt connection of lumped elements, since the ground plane is coplanar to the central (conductor) strip, and vias are not necessary. Nevertheless, in asymmetric CPW structures, such as bended lines, or asymmetrically loaded (along its length) lines, or in CPW lines with discontinuities, the parasitic slot mode[29] may be generated and obscure the fundamental mode (and hence degrade device performance). To prevent the presence of the slot mode in asymmetric CPW transmission lines, the ground plane regions must be electrically connected through air bridges, or by means of backside strips and vias (this technique has been applied to many CPW-based artificial transmission lines and microwave devices based on them, as will be seen along this book).

In CPWs, the transverse line geometry (see Fig. 1.2) is determined by the strip, W, and slot, G, widths (and of course by the substrate thickness, h, which is not usually a design parameter). Therefore, the characteristic impedance does not univocally determine the transverse line dimensions (W and G). This flexibility in the lateral geometry can be of interest in some applications. Moreover, for a given substrate thickness, it is possible to achieve higher characteristic impedances in CPW technology as compared to microstrip lines, where the strip width is univocally determined by the impedance value.

Suspended microstrip lines can be implemented by using sustaining posts in order to create an air gap between the ground plane and the substrate, or by means of advanced micromaching technologies [18], where the (lossy) substrate is partly removed by etching. As compared to conventional microstrip lines, suspended microstrip lines are thus low-loss lines. Moreover, because most of the field is in the air gap, higher characteristic impedances can be realized. Additionally, the presence of the air gap reduces the effects of dispersion, and such lines are of special interest in the upper microwave and lower millimeter wave bands. However, despite these beneficial properties, suspended microstrip lines are difficult to implement, and their use is restricted to applications where the required performance justifies the higher fabrication costs, or to monolithic microwave integrated circuits (MMICs). A modification of the suspended microstrip line is the so-called inverted microstrip line, where the conductor strip is placed below the substrate, in contact with the air gap. The advantages and drawbacks are similar to those of the suspended microstrip line.

[29] The slot mode of a CPW is, in general, an undesired mode of odd nature, that is, the symmetry plane of the CPW transmission line is an electric wall (or a virtual ground) for this mode. Conversely, the symmetry plane is a magnetic wall for the fundamental (even) CPW mode.

Slot lines are transmission lines that can be used either alone or in combination with microstrip lines on the opposite side of the substrate [19, 20]. Resonant slots coupled to microstrip lines have been used for the implementation of stop band filters, and slot antennas, consisting of a resonant slot fed by a microstrp line, are very well known [21]. For guided wave applications, radiation must be minimized. This is achieved through the use of high permittivity substrates, which causes the slot-mode wavelength to be small compared to free-space wavelength, and thereby results in the fields being closely confined to the slot with negligible radiation loss. The slot line shares with the CPW the coplanar configuration; hence, slot lines are especially convenient for shunt connecting lumped elements. Like microstrip lines or CPWs, slot lines do not support purely TEM modes. Indeed, the slot mode is markedly a non-TEM mode, and hence the characteristic impedance and the phase velocity in the slot line vary with frequency [19] (in contrast to microstrip lines or CPWs, where the line parameters are constant to a first-order approximation).

Except the slot line, the planar transmission lines considered earlier are single-ended (or unbalanced) lines. However, in applications where high immunity to noise, low crosstalk, and low electromagnetic interference (EMI) are key issues (i.e., in high-speed digital circuits), balanced (or differential) lines, and circuits are of primary interest. In two-conductor unbalanced transmission lines, the conductors have different impedance to ground, as sketched in Figure 1.11a. Such lines are fed by single-ended ports in which there is an active terminal and a ground terminal (i.e., one of the conductors is fed whereas the other is tied to ground potential). One of the conductors transports the signal current and the other acts as the return current path. By contrast, in two-conductor balanced lines (Fig. 1.11b), the conductors have equal potential with respect to ground and are in contra phase, and the currents flowing in the conductors have equal magnitude but opposite direction (each conductor provides the signal return path for the other). Such balanced lines are fed by a differential port, consisting of two terminals, neither of which being explicitly tied to ground. In balanced lines, the conductors have the same impedance to ground, this being the main relevant difference compared to unbalanced lines. Microstrip lines, CPWs, and striplines are examples of unbalanced lines. By contrast, slot lines, or coplanar strips (CPS), are balanced structures by nature. However, these balanced structures can be regarded as either balanced or unbalanced, depending on whether the excitation is balanced or unbalanced, respectively. Two-conductor balanced transmission lines can also be implemented by etching parallel strips at both sides of a dielectric slab

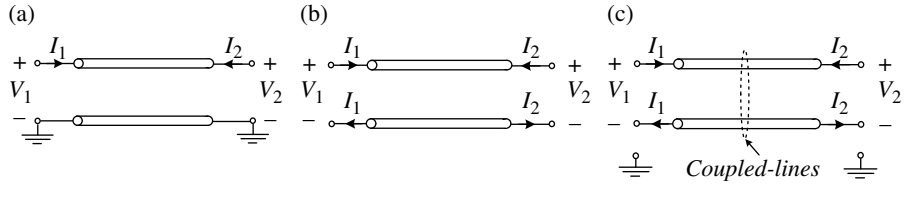

FIGURE 1.11 Schematic of two-port transmission lines. (a) Two-conductor unbalanced line, (b) two-conductor balanced line, and (c) three-conductor balanced line.

(see Fig. 1.2). This paired strips transmission line is useful, for instance, to feed antipodal printed dipole antennas [22]. Notice that the symmetry plane of the paired strips transmission line is an electric wall, and hence a virtual ground. Therefore, this structure can be analyzed by applying symmetry properties, that is, by removing the lower half of the structure, and adding a conducting plate, acting as ground plane, in the backside of the "sliced" substrate. Obviously, the resulting structure is a single-ended microstrip transmission line, and hence the main line parameters are calculated by applying the same formulas. However, the voltage drop across the paired strips is twice the voltage drop in the microstrip transmission line, whilst the current is the same. This means that the characteristic impedance of the balanced paired strips line is twice the characteristic impedance of the microstrip line.

Most practical implementations of balanced lines incorporate a ground plane, or some other global reference conductor. Such differential structures cannot be considered as pure two-conductor systems, since the ground plane becomes the third conductor of a three-conductor line (Fig. 1.11c). Such three-conductor line can be implemented by means of a pair of coupled lines over a ground plane. If the three-conductor line is not balanced due to the ground plane, currents flowing on it can unbalance the currents in the lines. On the contrary, if the three-conductor line is balanced, the active lines carry equal and opposite currents because the impedances of either line to ground are equal (see Fig. 1.11c). For instance, although a microstrip line is unbalanced, a two-port differential microstrip line can be designed by means of symmetric coupled lines (illustrated in Fig. 1.2—coupled microstrip) differentially driven. This balanced line consists of edge coupled lines that can be seen as a CPS line with a ground plane.

1.6 SOME ILLUSTRATIVE APPLICATIONS OF PLANAR TRANSMISSION LINES

There are several textbooks focused on the analysis and design of planar distributed circuits and antennas. Our aim in this Section is not to review all these transmission line applications, but to simply discuss some examples of distributed circuits where the involved transmission lines and stubs operate at different regimes, i.e., have different electrical lengths at the frequencies of interest. This includes planar circuits based on semi-lumped transmission lines (i.e., transmission lines with length $l < \lambda/10$), and based on $\lambda/8$, $\lambda/4$ and $\lambda/2$ lines. Some of the implementations reported in this Section will be later designed by means of artificial transmission lines in order to reduce circuit size, improve circuit performance, or achieve novel functionalities (or a combination of the previous beneficial aspects).

1.6.1 Semilumped Transmission Lines and Stubs and Their Application to Low-Pass and Notch Filters

Let us start by considering the design of circuits on the basis of electrically small planar components, usually referred to as semilumped components. The characteristic

dimension[30] of these components is typically smaller than $\lambda/10$ at the frequency of interest. The main relevant characteristic of semilumped components is the fact that they can be described by simple reactive elements, such as inductors, capacitors, or LC resonant tanks, up to frequencies satisfying the semilumped element approximation ($l < \lambda/10$). Let us consider an electrically small ($l < \lambda/10$) section of a transmission line, with electrical length βl and characteristic impedance Z_o. From (1.6), we can write

$$\beta l = \omega l \sqrt{L'C'} \tag{1.91}$$

The previous equation can be expressed in terms of the characteristic impedance and the per-unit-length inductance of the line as follows:

$$\beta l = \omega l \sqrt{L'C'} = \omega l \frac{L'}{Z_o} \tag{1.92}$$

or as a function of the characteristic impedance and the per-unit-length line capacitance according to

$$\beta l = \omega l \sqrt{L'C'} = \omega l Z_o C' \tag{1.93}$$

Thus, the line inductance and capacitance of the considered transmission line section can be expressed as follows:

$$L\omega = Z_o \beta l \tag{1.94a}$$

$$C\omega = \frac{\beta l}{Z_o} \tag{1.94b}$$

Equations 1.94 reveal that if the line is electrically short and Z_o is high, the capacitance of the considered transmission line section can be neglected and hence the line is essentially a series inductance; conversely, for an electrically short low impedance line, the line can be described by a shunt capacitance (the line inductance can be neglected). At first sight, one may erroneously deduce from (1.94) that the electrically short line condition (semilumped approximation) is not a requirement to describe the line by means of a series inductance or a shunt capacitance (very high/low value of Z_o leads to a negligible line capacitance/inductance). However, the line is not free from distributed effects (despite the fact it has an extreme—high or low—characteristic impedance) if it is not electrically short. If the line is electrically short, expressions (1.33) can be approximated by

[30] By characteristic dimension we mean the length (for a transmission line section or stub), the diameter (for a circular semilumped component, such as a circularly shaped split ring resonator or SRR), or the longest side length (for a rectangular planar component, such as a folded stepped impedance resonator or SIR). The analysis of these electrically small resonators and their applications will be considered later.

$$Z_{\text{in}}(Z_{\text{L}} = \infty) = -j\frac{Z_{\text{o}}}{\beta l} = -j\frac{1}{C\omega} \tag{1.95a}$$

$$Z_{\text{in}}(Z_{\text{L}} = 0) = jZ_{\text{o}}\beta l = jL\omega \tag{1.95b}$$

where (1.94) has been used. Hence, it is demonstrated that an electrically small transmission line section with extreme characteristic impedance can be described either by a series inductor or by a shunt capacitor, and the element values can be inferred from (1.94).[31]

From the previous words, it follows that by cascading electrically small transmission line sections with high and low characteristic impedance, we can implement a ladder network with series inductances and shunt capacitances, that is, a low-pass filter. The design procedure simply consists of setting the high and low characteristic impedance to implementable values, and determining the line length l of each transmission line section by means of (1.94) [1]. Notice that the higher/lower the characteristic impedance, the shorter the resulting inductive/capacitive transmission line section. After calculation, it is necessary to verify that each transmission line section satisfies the semilumped element approximation. An illustrative example of a stepped impedance low-pass filter (in CPW technology) and its frequency response are presented in Figure 1.12. The device is a ninth-order Butterworth low-pass filter with a cut-off frequency of $f_{\text{c}} = 2$ GHz (the element values of the filter are inferred from impedance and frequency transformation from the low-pass filter prototype [1]). The widths of the central strips and slots for the different sections are obtained by means of a transmission line calculator, once the characteristic impedance of the high- and low-impedance transmission line sections is set. Such calculators incorporate the formulas that link the lateral line geometry to the characteristic impedance, present in most textbooks focused on transmission lines [6].

In microwave engineering, shunt- and series-connected resonators (either distributed or semilumped) are key elements. In particular, shunt-connected series resonators introduce transmission zeros (notches) in the frequency response, which are of interest for harmonic suppression, or to improve the selectivity in microwave filters (elliptic low-pass filters are implemented by means of shunt resonators in order to generate transmission zeros above the pass band of interest). An open-ended shunt stub behaves as a parallel connected series resonator in the vicinity of the frequency that makes the line to be $\lambda/4$ long. However, the stub length can be significantly reduced by considering a stepped impedance topology, as depicted in Figure 1.13 [23]. Such element is known as stepped impedance shunt stub (SISS) and is described by a grounded series resonator. The narrow (high impedance) and wide (low impedance) transmission line sections correspond to the inductance and capacitance, respectively. The admittance of the SISS (seen from the host line) is given by

[31] Alternatively, expressions (1.94) and the semilumped approximation requirement have been derived by considering the equivalent T-circuit model of a transmission line section, where the series and shunt impedance are calculated from the elements of the impedance or admittance matrix [1].

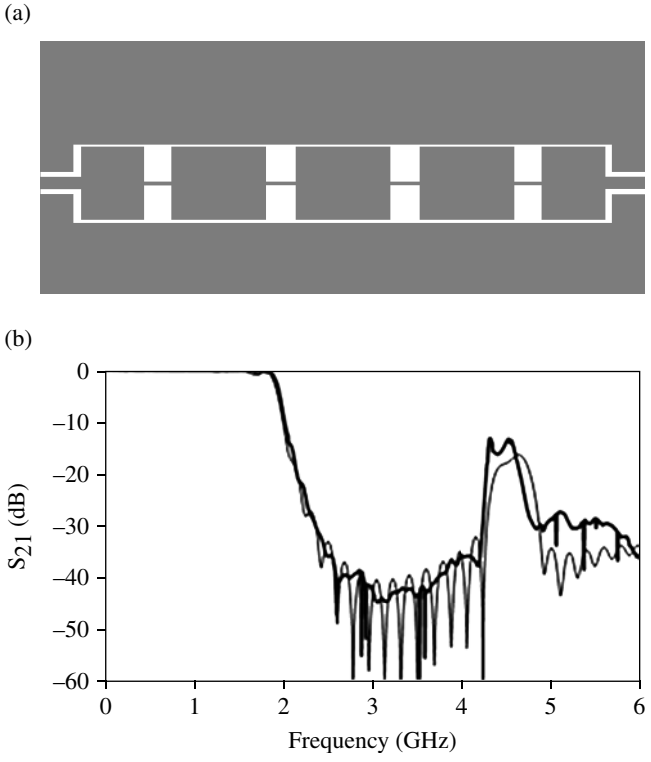

FIGURE 1.12 Order-9 Butterworth stepped impedance low-pass filter (a) and measured (solid line) and EM simulated (thin line) frequency response (b). The filter was fabricated on the *Rogers RO3010* substrate with dielectric constant $\varepsilon_r = 10.2$, and thickness $h = 1.27$ mm. Filter length is 9.4 cm.

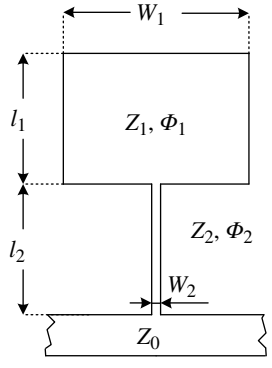

FIGURE 1.13 Topology of the SISS in microstrip technology and relevant dimensions ($Z_2 \gg Z_1$).

$$Y_{\mathrm{SISS}} = -j\frac{\tan\phi_1 + K\tan\phi_2}{Z_2\tan\phi_1\cdot\tan\phi_2 - Z_1} \tag{1.96}$$

where ϕ_1 and ϕ_2 are the electrical lengths of the low- and high-impedance line sections, respectively, and

$$K = \frac{Z_1}{Z_2} \tag{1.97}$$

is the impedance ratio of the SISS [24]. At resonance, the denominator in (1.96) vanishes, and the following condition results[32]:

$$K = \tan\phi_1\cdot\tan\phi_2 \tag{1.98}$$

It is obvious from (1.98) that to minimize the total electrical length ($\phi_{\mathrm{T}} = \phi_1 + \phi_2$) of the resonator, K must be as small as possible ($K \ll 1$) [24]. The reduction of ϕ_{T} is important for two reasons: (1) to reduce the length of the SISS and (2) to be able to describe the SISS by means of a lumped element model (grounded series LC resonator) over a wide frequency band. Under the assumption that the two transmission line sections of the SISS are electrically small, the tangents in (1.96) can be linearized, and the admittance of the SISS is found to be

$$Y_{\mathrm{SISS}} = -j\frac{\phi_1 + K\phi_2}{Z_2\phi_1\phi_2 - Z_1} \tag{1.99}$$

This admittance is identical to that of an LC series resonant tank, given by

$$Y_{\mathrm{LC}} = -j\frac{\omega C}{LC\omega^2 - 1} \tag{1.100}$$

provided the following mapping is satisfied:

$$C = \frac{l_1}{v_{\mathrm{p1}}Z_1} + \frac{l_2}{v_{\mathrm{p2}}Z_2} = C_1 + C_2 \tag{1.101}$$

$$L = \frac{Z_2 l_2}{v_{\mathrm{p2}}}\frac{\dfrac{l_1}{v_{\mathrm{p1}}Z_1}}{\dfrac{l_1}{v_{\mathrm{p1}}Z_1} + \dfrac{l_2}{v_{\mathrm{p2}}Z_2}} = L_2\frac{C_1}{C_1 + C_2} \tag{1.102}$$

[32] Notice that if $K = 1$, the resonance condition (1.98) rewrites as $\tan(\phi_1 + \phi_2) = \infty$, giving $\phi_{\mathrm{T}} = \phi_1 + \phi_2 = \pi/2$, that is, a $\lambda/4$ open stub at resonance. This result is easily inferred by applying the following trigonometric identity to (1.96): $\tan(\phi_1 + \phi_2) = (\tan\phi_1 + \tan\phi_2)/(1 - \tan\phi_1\cdot\tan\phi_2)$.

where v_{p1} and v_{p2} are the phase velocities of the low- and high-impedance transmission line sections, respectively, C_1 and C_2 are the line capacitances, namely,

$$C_1 = \frac{l_1}{v_{p1} Z_1} = C_1' \cdot l_1 \tag{1.103}$$

$$C_2 = \frac{l_2}{v_{p2} Z_2} = C_2' \cdot l_2 \tag{1.104}$$

C'_i $(i = 1, 2)$ being the per unit length capacitances of the lines, and L_2 is the inductance of the high impedance transmission line section, that is,

$$L_2 = L_2' \cdot l_2 \tag{1.105}$$

Notice that although C is dominated by the capacitance of the low impedance transmission line section, C_1, the contribution of C_2 on C may be nonnegligible if either K or l_2 are not very small. It is also interesting to note that L is somehow affected by the capacitive line section, such inductance being smaller than the inductance of the high-impedance transmission line section, L_2. Obviously, to a first-order approximation, the resonator elements are given by $C \approx C_1$ and $L \approx L_2$ (as expected on account of 1.95), although this approximation sacrifices accuracy.

Figure 1.14 shows the photograph of a SISS resonator loading a 50 Ω microstrip transmission line, where $L = 3.7$ nH and $C = 6.9$ pF (the resonance frequency is $f_o = 1$ GHz [23]). The impedance of the inductive line is that corresponding to a line width of 150 μm, namely, $Z_2 = 101.8$ Ω (the structure is implemented on the *Rogers RO3010* substrate with dielectric constant $\varepsilon_r = 10.2$ and thickness $h = 1.27$ mm). For the low-impedance transmission line section, the width (23 mm) guarantees that the first transverse resonance occurs beyond $2f_o$ (see details in Ref. [25]). This gives a characteristic impedance of $Z_1 = 5.8$ Ω. The lengths of the lines, $l_1 = 2.8$ mm and $l_2 = 4$ mm, were derived from (1.101) and (1.102) (actually some optimization was required due to the effects of line discontinuities, not accounted for by the model). These line lengths correspond to electrical lengths of $\phi_1 = 20.7°$ and $\phi_2 = 23.8°$ at $2f_o$. The EM simulation and the measured frequency response of the SISS-loaded line is also depicted in Figure 1.14. The circuit simulation of the same line loaded with a shunt connected LC resonator with the reactive values given above is also included in the figure, for comparison purposes. The agreement is excellent up to $2f_o$, indicating that the semilumped approximation is valid in the considered frequency range. Although, typically, notch filters (i.e., stop band filters with a peaked response, or transmission zero) exhibit narrow stop bands, the structure of Figure 1.14 can be considered to belong to this category (the bandwidth can be controlled by the inductance/capacitance ratio).

To end this subsection devoted to semilumped transmission lines and components, let us briefly consider the stepped impedance resonator (SIR) [26], which consists of a pair of wide transmission line sections sandwiching a narrow strip (Fig. 1.15a). This resonator is electrically smaller than the conventional $\lambda/2$ resonator (in the same form

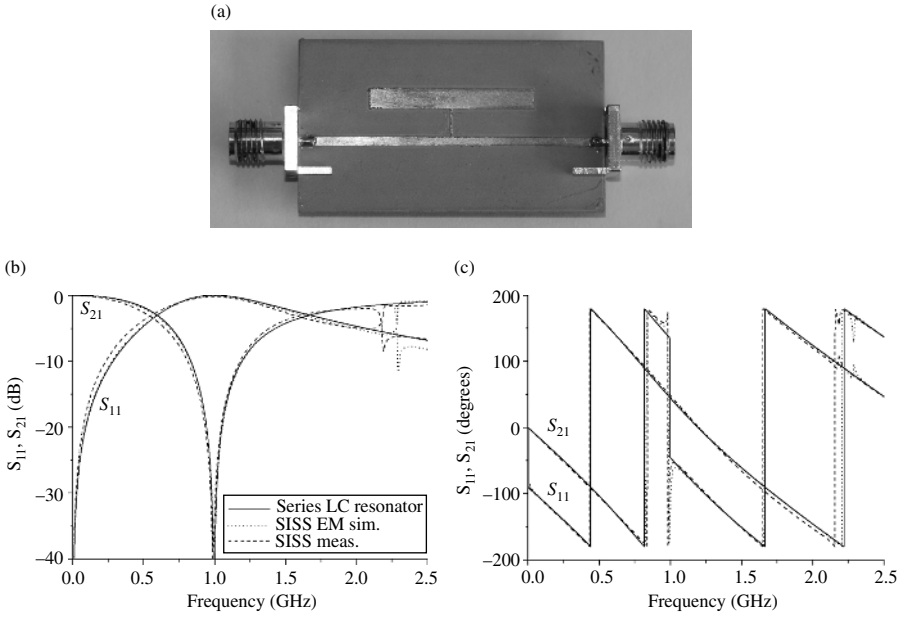

FIGURE 1.14 SISS-loaded microstrip line (a), insertion and return loss (b) and phase response (c). Reprinted with permission from Ref. [23]; copyright 2011 IET.

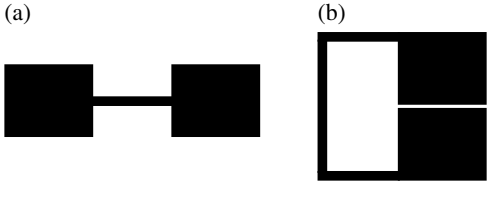

FIGURE 1.15 Topology of a SIR (a), and folded SIR (b).

than the SISS is electrically smaller than the $\lambda/4$ open stub). SIRs are typically driven through electric coupling, though they can also be externally driven by means of a time varying magnetic field by simply folding the SIR topology, as shown in Figure 1.15b. The size of the folded SIR can be further reduced by decreasing the gap distance between the wide transmission line sections, since this introduces an extra capacitance to the structure. SIRs have been used in a wide variety of microwave applications, including applications involving artificial transmission lines (as will be later shown). To illustrate the potentiality of these resonators, an SIR-based order-3 elliptic-function low-pass filter is reported (see further details in Ref. [27]). The filter is based on a CPW transmission line loaded with an SIR etched in the back substrate side. The wide strip sections of the SIR are placed face-to-face with the central strip and ground plane of the CPW host line, resulting in a shunt connected series resonator which introduces a transmission zero. The circuit model of an elliptic low-pass filter

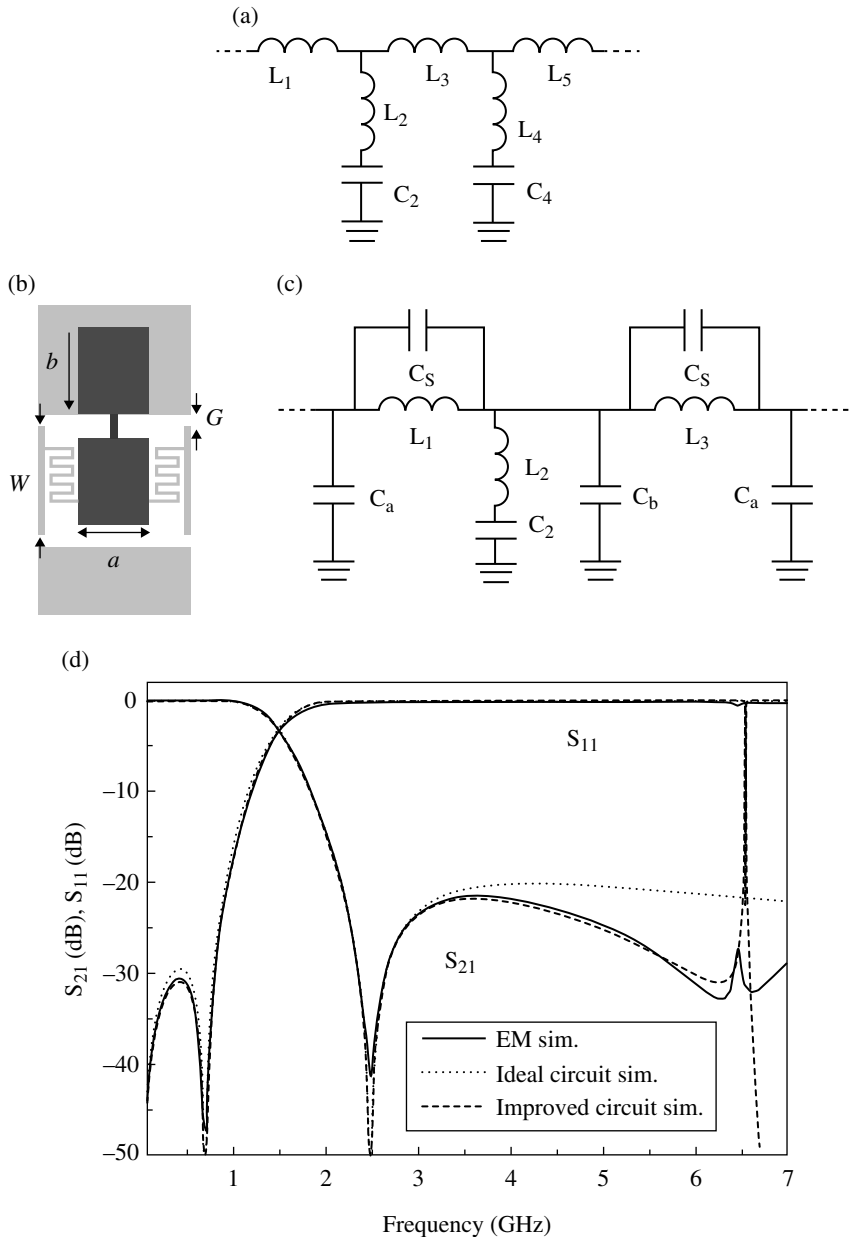

FIGURE 1.16 (a) Low-pass elliptic-function prototype filter with shunt connected series resonators (the circuit correspond to a fifth-order prototype), (b) topology of the SIR-based low-pass filter (order-3), (c) equivalent circuit model including parasitics, and (d) EM response, ideal filter prototype response and circuit response including parasitics. The considered substrate thickness and dielectric constant are $h = 254\,\mu m$ and $\varepsilon_r = 11.2$, respectively. Dimensions are $W = 5$ mm, $G = 0.55$ mm, $a = 3.24$ mm, $b = 3.99$ mm. Back side metal is indicated in black colour. The element values of the ideal prototype filter shown in (a) are $L_1 = L_3 = 4.7$ nH, $L_2 = 1.38$ nH, $C_2 = 2.98$ pF. The element values of the complete circuit model in reference to the circuit shown in (c) are $L_1 = L_3 = 4.7$ nH, $L_2 = 1.65$ nH, $C_2 = 2.5$ pF, $C_a = 0.08$ pF, $C_b = 0.44$ pF, $C_s = 0.115$ pF. With regard to parasitics, C_s models the capacitance associated to the meander, and C_a, C_b are the capacitances from the central strip to the ground plane. Reprinted with permission from Ref. [27]; copyright 2010 IEEE.

based on shunt connected series resonators,[33] the proposed order-3 SIR-based filter, its circuit model including parasitics, and the frequency response, are depicted in Figure 1.16. The remarkable aspects of these SIR-based filters are the small size, and the excellent agreement between the ideal filter response (ideal circuit simulation) and the EM simulation up to frequencies above the transmission zero frequency. At higher frequencies, the parasitics must be included for an accurate description of the filter response (indicated as improved circuit simulation in the figure). Elliptic function low-pass filters using SISS in microstrip technology have also been reported [28].

1.6.2 Low-Pass Filters Based on Richard's Transformations

Let us now consider the potential of $\lambda/8$ open and short-circuit stubs, which are electrically larger than the semilumped components considered in the previous section. According to Richard's transformations, such stubs can be used to replace shunt inductors and capacitors. Let us illustrate their application to the implementation of low-pass filters. The key idea is to force the length of the stubs to be $\lambda/8$ at the filter cut-off frequency, ω_c. Using (1.35), the reactance of the short-circuit and open-circuit stub at ω_c is forced to be identical to that of the inductor and capacitor, respectively. Below that frequency, we also expect a similar reactance because the stubs have roughly a linear dependence with frequency. However, discrepancies between the reactances of the stubs and lumped elements are expected above ω_c.[34] Let us consider the implementation of an order-3 Chebyshev low-pass filter with a cut-off frequency of $f_c = 2$ GHz, and 0.5 dB ripple. From impedance and frequency transformation from the low-pass filter prototype, the series inductances and the shunt capacitance of the filter are $L_1 = L_3 = 6.35$ nH, and $C_2 = 1.74$ pF, respectively. Application of (1.35) gives $Z_{o1,3} = 79.8\ \Omega$ and $Z_{o2} = 45.6\ \Omega$, for the inductive and capacitive stubs, respectively. Since the implementation of series stubs is complex, at least in microstrip technology, let us replace the inductive stubs with shunt stubs. To this end, the Kuroda identity shown in Figure 1.17 is used [1].[35] To apply the Kuroda identity of Figure 1.17, we first cascade a pair of $\lambda/8$ long $50\ \Omega$ transmission line sections at the input and output port of the filter. Notice that this has effects on the phase response of the filter, but not on the magnitude of the insertion and return loss. Application of the Kuroda identity leads to the circuit of Figure 1.18. The layout of this filter, for microstrip technology considering the *Rogers R04003C* substrate with dielectric constant $\varepsilon_r = 3.38$ and thickness $h = 0.81$ mm, is also depicted in the Figure. The EM simulation of the filter response is compared with the ideal Chebyshev filter response, where it can be appreciated that the agreement is excellent up to the

[33] Alternatively, elliptic-function lowpass filters can be implemented by cascading series connected parallel resonators and shunt capacitors.

[34] Since the reactance of the stubs is a periodic function with frequency, the frequency response of the filter is also a periodic function, and spurious (or harmonic) bands are generated.

[35] Kuroda's identities are equivalences between two-port networks containing series- or shunt-reactive elements and transmission line sections (called unit elements), that are used to physically separate transmission line stubs, to transform series stubs into shunt stubs, and to change unrealizable characteristic impedances into implementable ones.

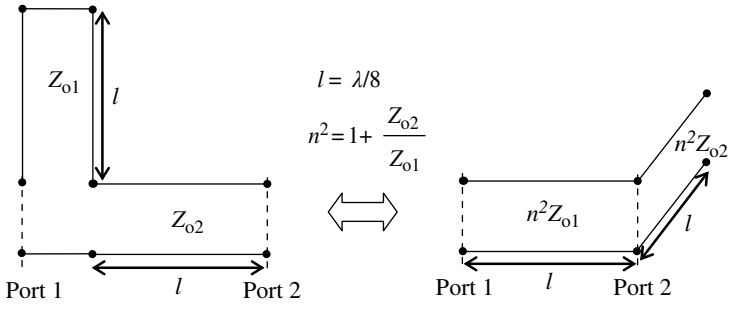

FIGURE 1.17 Kuroda identity used for the design of the filter of Figure 1.18.

cut-off frequency, and the frequency selectivity of the distributed implementation is significantly better, although with the presence of spurious bands (the filter response repeats every 8 GHz), as predicted before.

1.6.3 Power Splitters Based on $\lambda/4$ Lines

Power splitters, combiners, and couplers are fundamental building blocks in RF/microwave engineering. Most of their simplest implementations as distributed circuits are based on $\lambda/4$ lines.[36] Let us, hence, illustrate the application of $\lambda/4$ lines to the implementation of power splitters (it will be later shown that these lines can be replaced with artificial lines in order to reduce splitter size and obtain dual-band functionality). Power splitters are reciprocal[37] three-port networks (or multiport networks if the number of output ports is higher than 2) with a matched input port, that is, there is not power return to this port if the output ports are terminated with matched loads. If the splitter is lossless, the scattering matrix (for the case of a 1:2 device) can be written in the general form [1]:

$$S = \begin{pmatrix} 0 & \alpha & \alpha \\ \alpha & \gamma & -\gamma \\ \alpha & -\gamma & \gamma \end{pmatrix} \tag{1.106}$$

[36] Power splitters can also be implemented by means of lumped resistive elements [1]. Such splitters ideally exhibit an infinite operational bandwidth, but they are lossy. By contrast, distributed splitters can be considered (to a first approximation) lossless, but their functionality is restricted to a certain band in the vicinity of the operational frequency.

[37] Reciprocal networks are defined as those networks verifying that the effects of a source, located at one port, over a load, located at another port, are the same if the source and load interchange the ports where they are connected [1]. In reciprocal networks, the scattering matrix is symmetric.

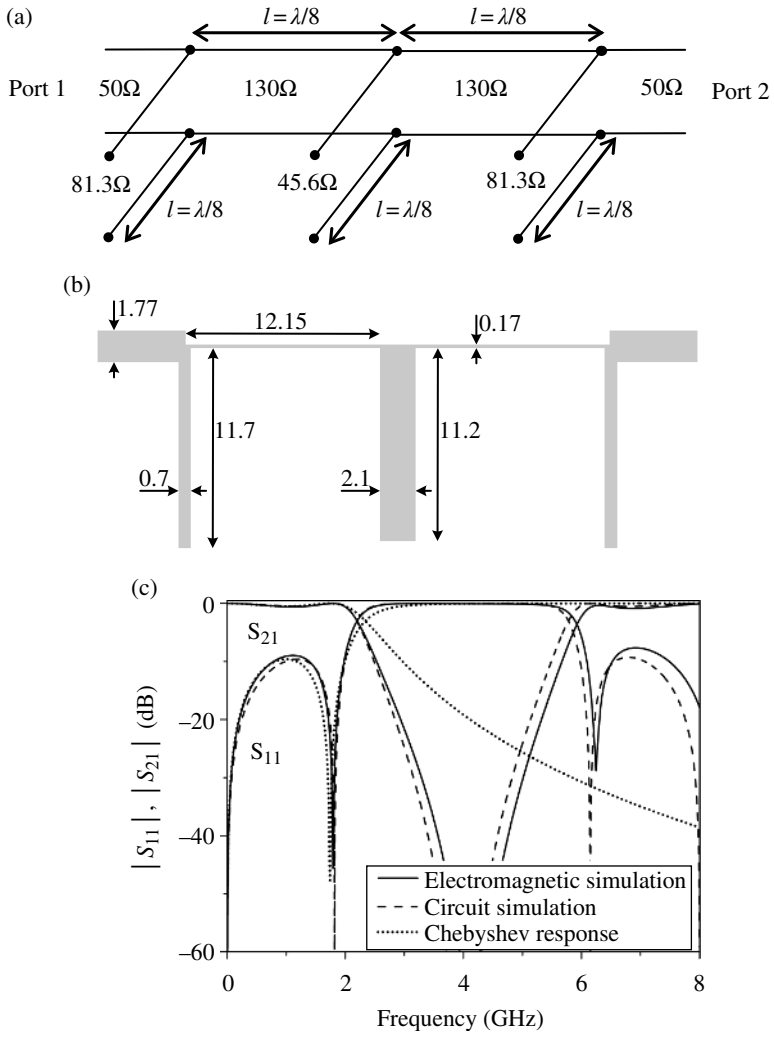

FIGURE 1.18 Schematic (a), layout (b), and frequency response (c) of the low-pass filter based on Richard's transformations. The relevant dimensions (in mm) are indicated. The circuit simulation in (c) was obtained by using a commercial circuit and schematic solver, where the transmission lines and stubs are modeled by the corresponding distributed models.

with $|\alpha| = 1/\sqrt{2}$ and $|\gamma| = 1/2$. The two canonical forms of lossless symmetric power splitters are depicted in Figure 1.19, where the impedances of the inverters ($\lambda/4$ lines), indicated in the figure, are derived by forcing the matching condition for the input port. In both implementations of Figure 1.19, $\alpha = -j/\sqrt{2}$, whereas $\gamma = 1/2$ for Figure 1.19a and $\gamma = -1/2$ for Figure 1.19b. The number of output ports of the splitter

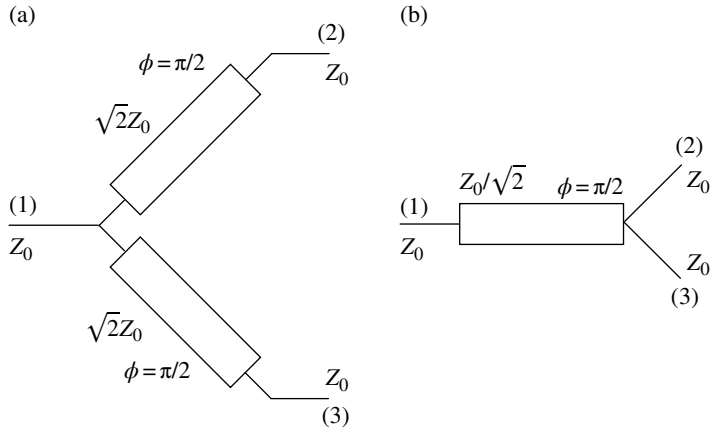

FIGURE 1.19 Canonical forms of the two-output distributed symmetric power splitter. (a) With two inverters and (b) with one inverter.

can be arbitrarily large. In order to preserve matching, the characteristic impedance of the inverters must be $Z_o = 50\sqrt{n}\Omega$ for the structure of Figure 1.19a and $50/\sqrt{n}\Omega$ for the structure of Figure 1.19b, where n is the number of output ports. A 1:3 power divider, corresponding to the configuration of Figure 1.19a, and its EM response are shown in Figure 1.20. The device was designed to be operative at 1.5 GHz, as revealed by the good matching at that frequency.

1.6.4 Capacitively Coupled $\lambda/2$ Resonator Bandpass Filters

The last illustrative example is a bandpass filter based on $\lambda/2$ transmission lines acting as distributed resonators. If a gap is etched on a transmission line, the frequency response is a high-pass type response, and this can be described by series connecting a capacitor to the line. However, if two capacitive gaps are etched in the line, rather than a high-pass response with enhanced rejection in the stop band, the structure exhibits a bandpass response that can be attributed to a resonance phenomenon. At the frequency where the distance between gaps is roughly $\lambda/2$, the forward and backward travelling waves (caused by gap reflections) in the resonator sum up in phase, and small coupling (and hence power transfer) between the feeding line and the resonator is enough to achieve total power transmission (assuming lossless lines) between the input and the output ports. Of course, this resonance phenomenon occurs at frequencies satisfying $l = n\lambda/2$ (with $n = 1, 2, 3, \ldots$).[38] Based on this phenomenon, bandpass filters with controllable response can be implemented (see Ref. [1] for further details on the design of this type of filters). As an example, an order-3 bandpass filter in

[38] Actually, this is the resonance condition for an unloaded resonator. The gaps introduce some phase shift in the reflected waves, and the resonance condition is slightly modified.

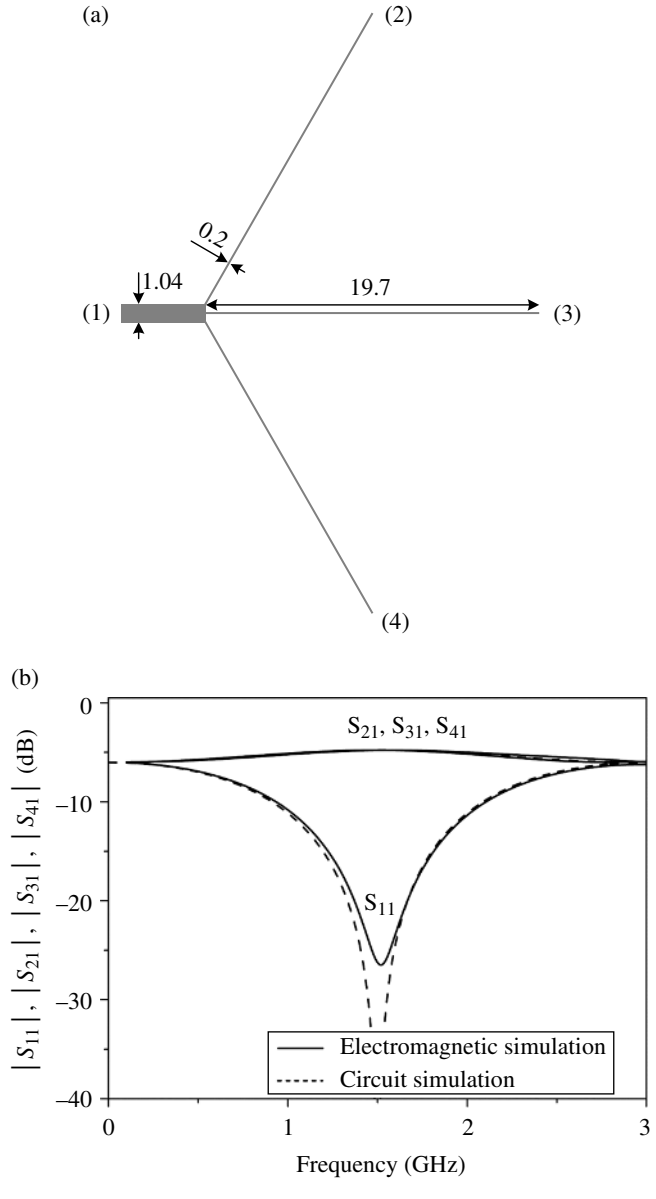

FIGURE 1.20 Example (layout) of a power splitter (a), and frequency response (b). Relevant dimensions (in mm) and device ports are indicated. The width of the three $\lambda/4$ lines gives a characteristic impedance of $Z_o = 50\sqrt{3} = 86.6\ \Omega$. The considered substrate is the *Rogers RO3010* with dielectric constant $\varepsilon_r = 10.2$ and thickness $h = 1.27$ mm.

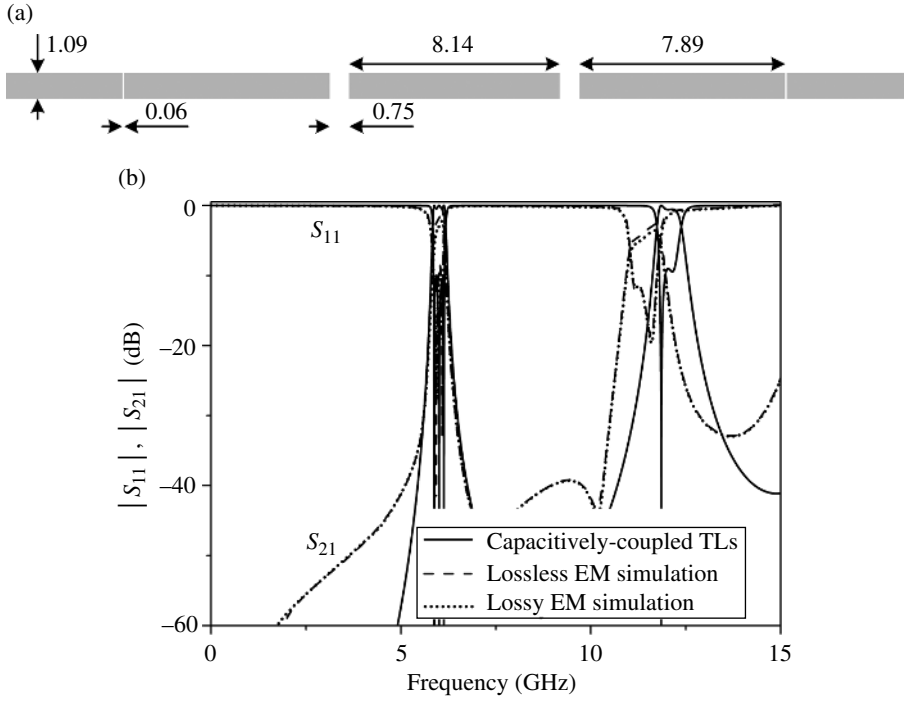

FIGURE 1.21 Example of a capacitively coupled $\lambda/2$ resonator bandpass filter (a) and frequency response (b). Relevant dimensions (in mm) are indicated. The considered substrate is the *Rogers RO3010* with dielectric constant $\varepsilon_r = 10.2$ and thickness $h = 1.27$ mm.

microstrip technology and its frequency response are shown in Figure 1.21. Resonator lengths and inter-resonators distance (i.e., gap space) have been calculated in order to obtain a Chebyshev response with 0.5 dB ripple, central frequency $f_o = 6$ GHz, and 5% fractional bandwidth (it will be shown in Chapter 2 that resonator's length can be reduced by means of slow wave artificial transmission lines).

REFERENCES

1. D. M. Pozar, *Microwave Engineering,* Addison Wesley, Reading, MA, 1990.
2. B. C. Wadell, *Transmission Line Design Handbook,* Artech House, Norwood, MA, 1991.
3. J. C. Freeman, *Fundamentals of Microwave Transmission Lines,* John Wiley, New York, 1996.
4. F. Di Paolo, *Networks and Devices Using Planar Transmission Lines,* CRC Press, Boca Raton, FL, 2000.
5. P. C. Magnusson, A. Weisshaar, V. K. Tripathi, G. C. Alexander, *Transmission Lines and Wave Propagation,* CRC Press, Boca Raton, FL, 2001.
6. I. Bahl and P. Barthia, *Microwave Solid State Circuit Design,* 2nd Edition, John Wiley, New York, 2003.

7. R. K. Mongia, I. J. Bahl, P. Barthia, and J. Hong, *RF and Microwave Coupled-Line Circuits,* 2nd Edition, Artech House, Norwood, MA, 2007.
8. L. Ganesan, and S. S. Sreeja Mole, *Transmission Lines and Waveguides,* 2nd Edition, McGraw Hill, New Delhi, 2010.
9. K. Kurokawa, "Power waves and the scattering matrix," *IEEE Trans. Microw. Theory Technol.*, vol. **MTT-13**, pp. 194–202, 1965.
10. P. I. Richards, "Resistor-transmission-line circuits," *Proc. IRE*, vol **36**. pp. 217–220, 1948.
11. S. Ramo, J. R. Whinnery, and T. Van Duzer, *Field and Waves in Communication Electronics,* 3rd Edition, John Wiley, New York, 1994.
12. R. A. Pucel, D. J. Massé, and C. P. Hartwig, "Losses in microstrip," *IEEE Trans. Microw. Theory Technol.*, vol. **MTT-16**, pp. 342–350, 1968.
13. G. Zou, H. Gronqvist, P. Starski, and J. Liu, "Characterization of liquid crystal polymer for high frequency system-in-a-package applications," *IEEE Trans. Adv. Packag.*, vol. **25**, pp. 503–508, 2002.
14. K. Chang, *Microwave Ring Circuits and Antennas,* John Wiley, New York, 1994.
15. L. Yang, A. Rida, and R. Vyas, M. M. Tentzeris "RFID tag and RF structures on a paper substrate using inkjet-printing technology," *IEEE Trans. Microw. Theory Technol.*, vol. **55**, pp. 2894–2901, 2007.
16. Association Connecting Electronics Industries. IPC TM-650 2.5.5.13. *Relative Permittivity and Loss Tangent Using a Split-Cylinder Resonator*. http://www.ipc.org/TM/2-5-5-13.pdf. Accessed February 5, 2015.
17. M. D. Janezic and J. Baker-Jarvis, "Full-wave analysis of a split-cylinder resonator for nondestructive permittivity measurements," *IEEE Trans. Microw. Theory Technol.*, vol. **47**, pp. 2014–2020, 1999.
18. C. T.-C. Nguyen, L. P. B. Katehi, and G. M. Rebeiz, "Micromachined devices for wireless communications," *Proc. IEEE*, vol. **86**, pp. 1756–1768, 1998.
19. S. B. Cohn, "Slot line on a dielectric substrate," *IEEE Trans. Microw. Theory Technol.*, vol. **MTT-17**, pp. 768–778, 1969.
20. K. C. Gupta, R. Carg, I. Bahl, and P. Barthia, *Microstrip Lines and Slotlines, 2nd Edition,* Artech House, Norwood, MA, 1996.
21. R. Garg, P. Bhartia, I. Bahl, and A. Ittipiboon, *Microstrip Antenna Design Handbook,* Artech House Inc., Norwood, 2001.
22. F. J. Herraiz-Martínez, F. Paredes, G. Zamora, F. Martín, and J. Bonache, "Dual-band printed dipole antenna loaded with open complementary split-ring resonators (OCSRRs) for wireless applications," *Microw. Opt. Technol. Lett.*, vol. **54**, pp. 1014–1017, 2012.
23. J. Naqui, M. Durán-Sindreu, J. Bonache, and F. Martín, "Implementation of shunt connected series resonators through stepped-impedance shunt stubs: analysis and limitations," *IET Microw. Antennas Propag.*, vol. **5**, pp. 1336–1342, 2011.
24. M. Makimoto and S. Yamashita, "Compact bandpass filters using stepped impedance resonators," *Proc. IEEE*, vol. **67**, pp. 16–19, 1979.
25. T. C. Edwards and M. B. Steer, *Foundations of Interconnect and Microstrip Design,* 3rd Edition, John Wiley, New York, 2000.
26. M. Makimoto and S. Yamashita, "Bandpass filters using parallel-coupled stripline stepped impedance resonators," *IEEE Trans. Microw. Theory Technol.*, vol. **MTT-28**, pp. 1413–1417, 1980.

27. M. Durán-Sindreu, J. Bonache, and F. Martín, "Compact elliptic-function coplanar waveguide low-pass filters using backside metallic patterns," *IEEE Microw. Wireless Compon. Lett.*, vol. **20**, pp. 601–603, 2010.

28. G. Matthaei, L. Young, and E.M.T. Jones, *Microwave Filters, Impedance Matching Networks, and Coupling Structures,* Artech House, Norwood, MA, 1980.